Climate of the Past Open Access
Discussions
EGU

The PMIP4-CMIP6 Last Glacial Maximum experiments: preliminary results and comparison with the PMIP3-CMIP5 simulations

Masa Kageyama[1], Sandy P. Harrison[2], Marie-L. Kapsch[3], Marcus Löfverström[4], Juan M. Lora[5], Uwe Mikolajewicz[3], Sam Sherriff-Tadano[6], Tristan Vadsaria[6], Ayako Abe-Ouchi[6], Nathaelle Bouttes[1], Deepak Chandan[7], Allegra N. LeGrande[8], Fanny Lhardy[1], Gerrit Lohmann[9], Polina A. Morozova[10], Rumi Ohgaito[11], W. Richard Peltier[7], Aurélien Quiquet[1], Didier M. Roche[1,12], Xiaoxu Shi[9], Andreas Schmittner[13], Jessica E. Tierney[4], Evgeny Volodin[14]

[1]Laboratoire des Sciences du Climat et de l'Environnement/Institut Pierre-Simon Laplace, UMR CEA-CNRS-UVSQ, Université Paris-Saclay, 91191 Gif-sur-Yvette, France

[2]School of Archaeology, Geography and Environmental Science (SAGES), University of Reading, UK

[3]Max-Planck-Institut für Meteorologie, 20146 Hamburg, Germany

[4]University of Arizona, Tucson, AZ 85721, USA

[5]Yale University, New Haven, CT 06520, USA

[6]Atmospheric and Ocean Research Institute, The University of Tokyo, Kashiwa, Japan

[7]Department of Physics, University of Toronto, 60 St. George Street, Toronto, Ontario M5S1A7, Canada

[8]NASA Goddard Institute for Space Studies, 2880 Broadway, New York, NY 10025, USA

[9]Alfred Wegener Institute, Bremerhaven, Germany

[10]Institute of Geography, Russian Academy of Science, Moscow, Russia

[11]Japan Agency for Marine-Earth Science and Technology, Yokohama, Japan

[12]Vrije Universiteit Amsterdam, Faculty of Science, Cluster Earth and Climate, de Boelelaan 1085, 1081HV Amsterdam, the Netherlands

[13]College of Earth, Ocean, and Atmospheric Sciences, Oregon State University, Corvallis, Oregon, USA

[14]Institute of Numerical Mathematics, Russian Academy of Sciences, Moscow, Russia

Correspondence to: Masa Kageyama (Masa.Kageyama@lsce.ipsl.fr)

Abstract. The Last Glacial Maximum (LGM, ~21,000 years ago) has been a major focus for evaluating how well state-of-the-art climate models simulate climate changes as large as those expected in the future using paleoclimate reconstructions. A new generation of climate models have been used to generate LGM simulations as part of the Palaeoclimate Modelling Intercomparison Project (PMIP) contribution to the Coupled Model Intercomparison Project (CMIP). Here we provide a preliminary analysis and evaluation of the results of these LGM experiments (PMIP4-CMIP6) and compare them with the previous generation of simulations (PMIP3-CMIP5). We show that the PMIP4-CMIP6 are globally less cold and less dry than the PMIP3-CMIP5 simulations, most probably because of the use of a more realistic specification of the northern hemisphere ice sheets in the latest simulations although changes in model configuration may also contribute to this. There are important differences in both atmospheric and ocean circulation between the two sets of experiments, with the northern and southern jet streams being more poleward and the changes in the Atlantic Meridional Overturning Circulation being less pronounced in the PMIP4-CMIP6 simulations than in the PMIP3-CMIP5 simulations. Changes in simulated precipitation patterns are influenced by both temperature and circulation changes. Differences in simulated climate between individual models remain large so, although there are differences in the average behaviour across the two ensembles, the new simulation results are not fundamentally different from the PMIP3-CMIP5 results. Evaluation of large-scale climate features, such as land-sea contrast and polar amplification, confirms that the models capture these well and within the uncertainty of the palaeoclimate reconstructions. Nevertheless, regional climate changes are less well simulated: the models underestimate extratropical cooling, particularly in winter, and precipitation changes. The spatial patterns of increased precipitation associated with changes in the jet streams are also poorly captured. However, changes in the tropics are more realistic, particularly the changes in tropical temperatures over the oceans. Although these results are preliminary in nature, because of the limited number of LGM simulations currently available, they nevertheless point to the utility of using paleoclimate simulations to understand the mechanisms of climate change and evaluate model performance.

Climate
of the Past
Discussions

1 Introduction

25   The climate of the Last Glacial Maximum (LGM, ~21,000 years ago) has been a focus of the Paleoclimate Modelling
Intercomparison Project (PMIP) since its inception. It is the most recent global cold extreme, and as such has been widely
documented and used for benchmarking state-of-the-art climate models (Braconnot et al., 2012; Harrison et al., 2014, 2015).
The increase in global temperature rise from the LGM until now (~4° to 6°C, Annan and Hargreaves, 2015; Friedrich et al.,
2016) is of the same order of magnitude as the increase projected by 2100 CE under moderate to high-end emission scenarios.
30   The LGM world was very different from the present one, with large ice sheets covering northern North America and
Fennoscandia, in addition to the Greenland and Antarctic ice sheets still present today. These additional ice sheets resulted in
a lowering of the global sea level by ~120 m, which induced changes in the land-sea distribution. The closure of the Bering
Strait and the exposure of the Sunda and Sahul shelves between southeast Asia and the maritime continent are the most
prominent of these changes in land-sea geography. Atmospheric greenhouse gases (GHGs) were lower than pre-industrial (PI)
35   values, leading to cooling in addition to that induced by the large ice sheets. The cooling is more pronounced in the high
latitudes than in the tropics, and greater over land than ocean. The polar amplification and the land-sea contrast signals
simulated by the previous generation of palaeoclimate simulations (PMIP3-CMIP5) are similar in magnitude (although
opposite in sign) to the signals seen in future projections and have been shown to be consistent with climate observations for
the historic period and reconstructions for the LGM (Braconnot et al., 2012; Izumi et al., 2013; Harrison et al., 2014, 2015).
40   However, while the models are able to represent the thermodynamic behaviour that gives rise to these large-scale temperature
gradients, they underestimate cooling on land, especially winter cooling, and overestimate tropical cooling over the oceans
(Harrison et al., 2014). Thus, one question to be addressed with the new PMIP4-CMIP6 simulations is whether there is any
improvement in capturing regional temperature changes. The large temperature changes at the LGM make this interval a
natural focus for efforts to constrain climate sensitivity, but attempts to do this using the PMIP3-CMIP5 simulations were
45   inconclusive (Schmidt et al., 2014; Harrison et al, 2014), in part because of the limited number of LGM simulations available,
and in part because of the limited range of climate sensitivity sampled by these models. Changes in model configuration have
resulted in several of the PMIP4-CMIP6 models having substantially higher climate sensitivity than the PMIP3-CMIP5
versions of the same models, and thus the range of climate sensitivity sampled by the PMIP4-CMIP6 models is much wider.
This provides an opportunity to re-examine whether the LGM could provide a strong constraint on climate sensitivity.

50

The atmospheric general circulation was strongly modified from its modern day conditions by changes in coastlines at low
latitudes (DiNezio and Tierney, 2013) and by the presence of the Laurentide and Fennoscandian ice sheets (e.g. Laîné et al.,
2009; Lofverstrom et al., 2014, 2016; Ullman et al., 2014; Beghin et al., 2015). These changes in circulation had an impact on
precipitation, which was reduced globally (Bartlein et al., 2011) but increased locally, for example in southwestern North

Climate
of the Past
Discussions

Open Access

EGU

55   American and in the Mediterranean region (e.g., Kirby et al., 2013; Beghin et al., 2016: Goldsmith et al., 2017; Lora et al., 2017; Lora, 2018; Lofverstrom and Lora, 2017; Lofverstrom, in review). The interplay between temperature-driven and circulation-driven changes in regional precipitation at the LGM represents a test of the ability of state-of-the-art models to simulate precipitation changes under future scenarios, where both thermodynamic (e.g. related to the Clausius-Clapeyron relationship) and dynamic (e.g. related to changes in the position of the storm-tracks and extent of the subtropical anticyclones)

60   effects contribute to changes in the amount and location of precipitation (e.g., Boos, 2012; Scheff and Freirson, 2012; Lora, 2018). Evaluation of the PMIP3-CMIP5 simulations showed that models underestimate the LGM reduction in mean annual precipitation over land (Harrison et al., 2014), reflecting the underestimation of temperature changes in the simulations (Li et al., 2013), and this resulted in an underestimation of the observed aridity (precipitation minus evapotranspiration). While the models reproduced circulation-induced changes in precipitation in western North America, they showed no increase in

65   precipitation south of the North American ice sheet and only limited impact on the precipitation of the circum-Mediterranean region (Harrison et al., 2014; Lora, 2018; Morrill et al., 2018). Thus, one question to be addressed with the new PMIP4-CMIP6 simulations is whether there is any improvement in capturing regional precipitation changes. One complication here is that most of the reconstructions used to evaluate the PMIP3-CMIP5 simulations were pollen-based and relied on statistical approaches that do not account for the direct impact of low CO_2 on water-use efficiency (Prentice and Harrison, 2009; Gerhardt

70   and Ward, 2010; Bragg et al., 2013; Scheff et al., 2017) and could therefore be dry biased. However, new methods have been developed that account for this effect (Prentice et al., 2017) and thus it will be possible to determine whether accounting for the effect of low CO_2 resolves model-data mismatches in regional precipitation at the LGM.

The LGM boundary conditions also had a strong impact on ocean circulation, as documented via multiple tracers (e.g. Lynch-

75   Stieglitz et al., 2007, Böhm et al., 2015) which suggest a shallower North Atlantic Deep Water cell and expanded Antarctic Bottom Water (AABW). This is at odds with the PMIP3-CMIP5 model results (Muglia and Schmittner, 2015) which all show an increase in the Atlantic Meridional Overturning Circulation (AMOC). Previous studies show that this increase in AMOC is related to changes in northern extratropical wind stress due to the presence of the high ice sheets (Oka et al. 2012, Muglia and Schmittner 2015, Klockmann et al. 2016, Sherriff-Tadano et al. 2018, Galbraith and de Lavergne 2019). Thus, the simulation

80   of the AMOC, and ocean circulation in general, at the LGM could be highly sensitive to the ice sheet reconstructions used as boundary conditions (see e.g. Ullman et al., 2014; Beghin et al., 2016). There is still some uncertainty about the height and shape (although not the extent) of the LGM ice sheets, so the protocol for the LGM PMIP4-CMIP6 experiment takes this uncertainty into account by allowing for alternate ice-sheet configurations (Kageyama et al., 2017) in order to test the sensitivity of LGM climate and ocean circulation to ice sheet configuration. The PMIP4-CMIP6 LGM experimental protocol

85   also includes changes in other forcings, including vegetation changes and changes in atmospheric dust loadings and their uncertainties. Thus, the new PMIP4-CMIP6 simulations provide opportunities to examine the response of the climate system to multiple forcings, to calculate the impact of individual forcings through sensitivity experiments, and to examine how these forcings combine to produce circulation and climate changes in the marine and terrestrial realms.

90 In this paper, we present preliminary results from the PMIP4-CMIP6 LGM simulations, compare them to the PMIP3-CMIP5 results (Section 3), and evaluate their realism against a range of climatic reconstructions (Section 4). We focus on temperature and precipitation, extratropical circulation, energy transport and the AMOC.

2 Material and methods

2.1 PMIP3-CMIP5 and PMIP4-CMIP6 protocols for the LGM simulations

95 The protocol of the LGM experiments changed between the PMIP3-CMIP5 and PMIP4-CMIP6 simulations (Kageyama et al., 2017), partly to accommodate new information about boundary conditions and partly to capitalise on new features of the climate models. The main difference between the PMIP3-CMIP5 and PMIP4-CMIP6 simulations is the specification of the ice sheets. The PMIP3-CMIP5 simulations all used the same ice sheet, which was created as a composite of three separate ice-sheet reconstructions (Abe-Ouchi et al., 2015); the PMIP4-CMIP6 protocol allows modelling groups to use one of three

100 separate ice-sheet reconstructions: the original PMIP3-CMIP5 ice sheet to facilitate comparison with the earlier simulations, ICE-6G_C (Argus et al., 2014, Peltier et al., 2015) and GLAC-1D (L. Tarasov, pers. comm.; Ivanovic et al., 2016). All three reconstructions have similar ice-sheet extent, but the height of the Laurentide, Fennoscandian, and West Antarctica ice sheets differ significantly, by several hundred metres in some places. Comparisons of the simulations made with alternative ice-sheet reconstructions will ultimately allow an assessment of the impact of forcing uncertainties on simulated climates.

2.2 PMIP3-CMIP5 and PMIP4-CMIP6 models

105 The LGM model output analysed here are from the PMIP4-CMIP6 and PMIP3-CMIP5 *lgm* experiments. We use the corresponding *piControl* experiments as a reference, which are termed "PI" throughout the manuscript. Seven PMIP4-CMIP6 LGM simulations are currently available, and there were a comparable number of models that ran LGM simulations in PMIP3-CMIP5 (Table 1). The PMIP3-CMIP5 ensemble includes one model that ran an additional sensitivity test to ice-sheet

110 height (GISS-E2R: Ullman et al., 2014) and one model that ran simulations with and without dynamic vegetation (MPI-ESM-P: Adloff et al., 2018). The PMIP4-CMIP6 ensemble includes two simulations made with updated versions of the models that contributed to PMIP3-CMIP5, specifically MIROC and MPI-ESM (Table 1). Most of the models that have run the PMIP4-CMIP6 LGM simulations are general circulation models (GCMs) but iLOVECLIM is an Earth System Model of Intermediate Complexity. As such, iLOVECLIM is considerably faster than the GCMs and is the only model so far that has

115 run simulations using different ice sheet reconstructions (ICE-6G_C and GLAC-1D). The LGM simulations were either initialised from a previous LGM simulation or were spun-up from the pre-industrial state. The length of the spin-up therefore varies (Table 1), as indeed does the length of the equilibrium LGM simulation in these preliminary analyses. The INM-CM4-8 results are from the beginning of an *lgm* simulation and the model is not yet fully equilibrated. All other models have run for several millennia. Our preliminary analyses are based on variables available by December 20th, 2019. Many modelling groups are in the process

120 of uploading data to the CMIP6 archive on the Earth System Grid Federation, but the minimum information we requested for this study were monthly surface air temperatures and precipitation. Although several of the PMIP4-CMIP6 have higher climate sensitivity than the equivalent models in PMIP3-CMIP5, this is not reflected in the ensemble analysed here. In fact, the PMIP4-CMIP6 ensemble, as of December 2019, has lower climate sensitivities than the PMIP3-CMIP5 models (Table 1): equilibrium sensitivities to a CO_2 doubling from pre-industrial values range from 2.1 to 3.6°C, (mean: 3.0°C) in the current PMIP4-CMIP6

125 ensemble, while the range is from 2.1 to 4.7°C (mean: 3.43°C) in the PMIP3-CMIP5 ensemble.

2.3 Sources of information on LGM climate

The PMIP3-CMIP5 model simulations were evaluated against two benchmark data sets: pollen-based reconstructions of seasonal temperature (mean annual temperature, mean temperature of the coldest month, mean temperature of the warmest month, and growing season temperature indexed by growing degree days above a baseline of 0°C), mean annual precipitation

130 and an index of soil moisture (Bartlein et al., 2011); and a compilation of sea-surface temperature (SST) reconstructions (MARGO, 2009).

In the Bartlein et al. (2011) data set, reconstructions at individual pollen sites were averaged to produce an estimate for a 2 x 2° grid; reconstruction uncertainties are estimated as a pooled estimate of the standard errors of the original reconstructions for

135 all sites in each grid cell. Although the Bartlein et al. (2011) has good coverage for some regions, coverage was sparse in the tropics, and there were no reconstructions of LGM climate for Australia. Furthermore, not all of the six climate variables were reconstructed at every site, so statistical comparisons were more robust for some variables that others. The majority of the reconstructions included in the Bartlein et al. (2011) data set used various sorts of statistical calibrations based on modern day conditions and therefore do not account for the impact that changes in CO_2 have on water-use efficiency and hence plant

140 distribution. Although Bartlein et al. (2011) were unable to demonstrate a statistically significant difference between statistical reconstructions and model-based inversions (which in principle account for the CO_2 effect on plant distribution), their analysis focused on the mid-Holocene where the CO_2 effect is small and there is therefore some concern that the data set may overestimate aridity at the LGM. Reconstructions which incorporate the effect of CO_2 are now available for Australia (Prentice et al., 2017). Cleator et al. (2019) have used 3D variational data assimilation techniques with a prior derived from the PMIP3-

145 CMIP5 LGM simulations and the Bartlein et al. (2011) and Prentice et al. (2017) pollen-based reconstructions, and incorporating the Prentice et al. (2017) CO_2 correction, to produce a new global reconstruction of terrestrial climate at the LGM. In addition to accounting for potential effects of low CO_2 on moisture variables at the LGM, this reconstruction produces coherent estimates of seasonal climate variables at many more points than the original pollen-based reconstructions and also extends the geographic coverage.

150

Tierney et al. (2019) provide a new synthesis of geochemical SST data ($U^{K'}_{37}$, TEX_{86}, Mg/Ca, and $d^{18}O$) from the LGM (19--23 ka) and the late Holocene (0--4 ka) time periods. This compilation builds upon the MARGO (2009) collection of $U^{K'}_{37}$ and

Climate
of the Past
Discussions

Mg/Ca data by including new studies published since MARGO was released, as well as expanding the collection to include TEX$_{86}$ and δ^{18}O of foraminifera. The Tierney et al. (2019) synthesis excludes microfossil-based SST estimates, on the basis

155 that: 1) these include no-analogue assemblages (Mix et al., 1999); 2) imply warmer-than-present subtropical gyres, an inference that has been questioned (Crowley, 2000; Telford et al., 2013); and 3) lack Bayesian proxy-system models that were required for the data assimilation technique used by Tierney et al. (2019). Tierney et al. (2019) use the data along with a model prior from the isotope-enabled Community Earth System Model 1.2 (Brady et al., 2019) to produce a full-field data assimilation product; however, since this product relies on the covariance structure of CESM, we only use the data synthesis for

160 comparisons here. Data from the LGM and late Holocene respectively were calibrated using Bayesian models that fully propagate uncertainties (Tierney & Tingley, 2015; Tierney et al., 2018; Malevich et al., 2019; Tierney et al., 2019), yielding a 1,000 member posterior distribution of SSTs. These data were sorted from low to high along the ensemble dimension, and then random error representative of site-level, downcore uncertainty (N(0,0.5˚C) was added back to the matrix. This procedure effectively partitions the error variance; i.e., it assumes that at any given site, absolute uncertainty in SST cancels out in the

165 anomaly calculation, while "relative" uncertainty associated with downcore measurement and non-linearities in the calibration model is preserved. The data were then averaged within a 5˚ x 5˚ grid and differenced. The standard deviation associated with each gridpoint is calculated from the differenced ensemble dimension. A crucial difference between the Tierney et al. (2019) synthesis and MARGO (2009) is that the former implies more extensive tropical cooling during the LGM (-2.5˚C, vs -1.5˚C for MARGO). This can be attributed to the exclusion of the microfossil data as well as recalibration of the U$^{K'}_{37}$ proxy with

170 the BAYSPLINE model (Tierney & Tingley, 2018), which corrects for an observed reduced sensitivity of U$^{K'}_{37}$ to SST above ca. 24˚ C.

2.4. Data-model comparisons

We compare the model simulations to palaeoclimate data, focusing on large-scale features and regional changes. In these

175 comparisons, the reconstructions are expressed as mean values and the uncertainty by the standard error of the reconstructions. Model outputs were extracted only for the grid cells where there are observations. Model uncertainty is represented by the standard deviation of interannual variability. Thus, model uncertainty is not, strictly speaking, equivalent to reconstruction uncertainty but merely provides some measure of the variability engendered by sampling the simulated climate.

180 **3 Model results**

3.1 Temperature

The global and annual mean temperature in the PMIP4-CMIP6 LGM simulations is between 3.5 and 4.1°C cooler than the PI simulations. The largest changes in temperature between the LGM and PI simulations (Fig. 1) is found over the Laurentide and Fennoscandian ice sheets, reflecting the significant changes in surface height and albedo caused by the ice sheets. Colder

185 conditions are registered in the northern mid and high latitudes, partly reflecting the advection of the cold temperature

anomalies downwind of the ice sheets. The cooling in the tropics, which results from both the lower atmospheric GHG concentrations and the remote influence of the northern ice sheets, is more muted. As expected, the simulations show larger changes over the land than over ocean. Zonally averaged temperatures (Fig. 2) confirm that the PMIP4-CMIP6 ensemble also shows the expected polar amplification of temperature changes in both northern and southern hemispheres.

190

Although the broadscale patterns of temperature changes are similar, there are important differences between the PMIP4-CMIP6 and PMIP3-CMIP5 ensembles. The PMIP4-CMIP6 simulations are generally warmer than the PMIP3-CMIP5 simulations (Fig. 1 bottom), except in regions close to West Antarctica, over some restricted areas of the Laurentide ice sheet and in the North Atlantic. The largest difference between the PMIP3-CMIP5 and PMIP4-CMIP6 averages is over the northern

195 North Atlantic and Nordic Seas, probably reflecting differences in sea-ice cover in these areas. Zonally averaged temperatures (Fig. 2) confirm the differences between the two sets of simulations. The northern extratropics are colder in the PMIP3-CMIP5 simulations (from -5 to nearly -13°C) than the PMIP4-CMIP6 simulations (from -5 to ca -9°C). Similarly, the PMIP3-CMIP5 simulations are slightly colder in the tropics (by -2.4 to -3.3 °C, with an outlier at -1.7°C) than the PMIP4-CMIP6 simulations (-1.7 to -2.6°C). However, the cooling of the southern extratropics is more variable in the PMIP4-CMIP6 simulations (-1.2 to

200 ca -7°C) than in the PMIP3-CMIP5 simulations (-2.5 to ca -6°C). Most of the difference in the global average cooling, which ranges from -3.5 to -4.1°C in the PMIP4-CMIP6 simulations and between -4.5 and -5.5°C in the PMIP3-CMIP5 simulations, stems from differences in the simulated temperatures of the northern hemisphere and probably reflect differences in the ice sheet reconstructions (e.g. Liakka and Lofverstrom, 2018) used in the two sets of simulations. However, it is also possible that differences in model configuration and in climate sensitivity could contribute to the difference between the two ensembles.

205 The PMIP4-CMIP6 ensemble is also small - only five models are included in the ensemble shown in Fig. 1 - and confirmation of whether differences in the temperature response of the two ensembles are real will only be possible when other LGM simulations become available.

3.2 Atmospheric and oceanic circulation

The PMIP4-CMIP6 models simulate large changes in the Northern Hemisphere upper tropospheric atmospheric circulation

210 (Fig. 3), in response to LGM boundary conditions, in particular over North America and the North Atlantic. The North Atlantic jet stream is narrower and stronger compared to the PI, as shown by an increase of more than 10 m/s in the 250 hPa zonal wind south of the Laurentide ice sheet and extending into the North Atlantic, and a decrease in zonal wind to the northwest and southeast of these regions. The strengthening and narrowing of the North Atlantic jet stream was also a characteristic of the PMIP3-CMIP5 simulations (Beghin et al., 2016). However, in the PMIP4-CMIP6 simulations the jet stream is further north

215 than in the PMIP3-CMIP5 simulations (Fig. 3, bottom), most prominently near the Laurentide ice sheet. This could be because the Laurentide is lower in the ICE-6G reconstruction than the ice sheet used in the PMIP3-CMIP5 simulations (see e.g. Ullman et al., 2014; Beghin et al., 2015; Lofverstrom et al., 2016) but may also reflect changes in the representation of the zonal winds between the two sets of simulations. This is supported by the fact that there are differences between the PMIP3-CMIP5 and

Climate
of the Past
Discussions

PMIP4-CMIP6 simulations away from the Laurentide ice sheet, in particular over the North Pacific and the Southern Ocean,
220 where the jet stream is also located more poleward in the PMIP4-CMIP6 than the PMIP3-CMIP simulations. Sensitivity
experiments using the PMIP3-CMIP5 ice sheets with PMIP4-CMIP6 models, as planned in the PMIP4 LGM experiment
protocol (Kageyama et al., 2017), should help resolve the question of whether differences in model treatment or boundary
conditions are responsible for the differences in atmospheric circulation between the two ensembles.

225 The extent of the North Atlantic Deep Water (NADW) cell simulated by PMIP4-CMIP6 models is very similar for LGM and
PI, except for iLOVECLIM, which shows a deepening of the NADW cell for LGM (Fig. 4, the data available for this analysis
are from the following models: UoT-CCSM4, AWIESM1, AWIESM2, MPI- ESM1.2, MIROC-ES2L and iLOVECLIM). Two
of the PMIP4-CMIP6 models show a deep NADW cell reaching the ocean floor in the North Atlantic, whereas four of the
PMIP4-CMIP6 models simulate some Antarctic Bottom Water (AABW) in the North Atlantic. UoT-CCSM4 even shows a
230 shallowing of the NADW cell for LGM. The intrusion of AABW cell into the North Atlantic was shown by some of the
PMIP3-CMIP5 simulations, but not as much as the PMIP4-CMIP6 simulations (Fig. 4 and Muglia et al., 2015). Four of the
PMIP3-CMIP5 models produced a NADW cell reaching the ocean floor in the North Atlantic, and only three had extensive
AABW. The maximum strength of the NADW cell itself strengthens in all of the PMIP4-CMIP6 simulations, by as much as
6 Sv. This strengthening is consistent with PMIP3-CMIP5 results and is likely to be associated with the vigorous surface wind
235 over the northern North Atlantic (Muglia and Schmittner 2015, Sherriff-Tadano and Abe-Ouchi 2020), and the closure of the
Bering Strait (Hu et al. 2015). The strength of the AMOC reduces south of 30°N in UoT-CCSM4. iLOVECLIM performed
simulations of LGM with two different ice sheet reconstructions (ICE6G, GLAC1D) and show a weaker NADW cell in
GLAC1D than that produced by ICE6G. This weakening may be associated with a lower topography of the ice sheet of
GLAC1D (e.g. Zhang et al. 2014). These circulation changes in the Atlantic Ocean are reflected in the total ocean heat transport
240 (Fig. 5, bottom, the PMIP4-CMIP6 results available for this analysis are from the MIROC-ES2L, MPI-ESM1.2, INM-CM4-8
and UoT-CCSM4 models). MPI-ESM1.2 simulates an increase in northward ocean heat transport at all latitudes for the LGM
compared to PI, while MIROC-ES2L simulates an increase in this transport from 15°S to 60°N. UoT-CCSM4 is the only
model simulating a decrease in northward heat transport over a significant range of latitudes, from 50°S to 70°N. All PMIP4-
CMIP6 models simulate an increase in northward atmospheric heat transport, in the tropics and up to 50°N. MIROC-ES2L
245 simulates an increase up to 70°N (Fig. 5, middle). In summary, all models simulate an increase in northward heat transport
(Fig. 5, top) in the tropics and northern mid-latitudes, although in the UoT-CCSM4 model the increase is confined to south of
50°N. This increase in northward heat transport in the tropics and northern mid-latitudes during the LGM as compared to PI
was also simulated by most PMIP3-CMIP5 models. Given that the magnitude of the heat transport increase is similar in the
PMIP4-CMIP6 and PMIP3-CMIP6 simulations, the warmer temperatures at high northern latitudes in the PMIP4-CMIP6
250 simulations cannot be due to differences in northward ocean heat transport.

Climate
of the Past
Discussions

EGU

3.3 Hydrological cycle

The large-scale gradients in precipitation are similar in the PMIP4-CMIP6 LGM and PI simulations (Fig. 6, top), with maximum precipitation in the tropics (Intertropical Convergence Zone and monsoon regions) and secondary maxima in the

255   mid-latitudes, corresponding to the position of the North Pacific, North Atlantic, and Southern Ocean storm-tracks. The PMIP4-CMIP6 models show a decrease in precipitation between the LGM and PI in all these high precipitation areas (Fig. 6, middle and Fig. 7, top left). There are some regions where precipitation increases at the LGM compared to the PI: all PMIP4-CMIP6 models simulate more precipitation over the Pacific Ocean and to the south of the Laurentide ice sheet, and over southern Africa; some models simulate wetter conditions over the Iberian Peninsula, and some simulate an increase in

260   precipitation over the northern and southern subtropical zones in the Pacific and over the Atlantic southern subtropical zone. However, the areas with decreased precipitation are much more extensive than areas with increased precipitation, so zonal averages for the southern extratropics, tropics and northern extratropics (Fig. 7) all show a decrease in precipitation.

The broadscale patterns of change in precipitation in the PMIP4-CMIP6 simulations are similar to those found in the PMIP3-

265   CMIP5 simulations. The PMIP4-CMIP6 ensemble is slightly less dry than the PMIP3-CMIP5 ensemble (Fig. 6), particularly in the northern extratropics, and this may reflect the fact that the PMIP4-CMIP6 simulations are less cold than the PMIP3-CMIP5 simulations. However, the geographic patterning in the precipitation changes between the PMIP4-CMIP6 and PMIP3-CMIP5 ensembles (Fig. 6, bottom) is complex, and some of the differences between the two ensembles are probably related to atmospheric circulation changes, particularly in the tropics (Fig. 3). Both ensembles show a consistent decrease in zonally

270   averaged precipitation in the southern extratropics, tropics, and northern extratropics (Fig. 7). When obvious outliers are excluded (e.g. CNRM-CM5 for PMIP3, iLOVECLIM for PMIP4), the simulated range of precipitation changes is comparable for the PMIP3-CMIP5 and PMIP4-CMIP6 ensembles.

Evapotranspiration patterns in the PMIP4-CMIP6 LGM and PI simulations are characterized by maximum values in the

275   subtropics and decreases toward high latitudes. The models simulate a global decrease in LGM evapotranspiration relative to the PI that strongly peaks over and around the northern hemisphere ice sheets (Fig. 8, left). These results are in agreement with the broad patterns of the PMIP3-CMIP5 ensemble, albeit with a muted average decrease consistent with the fact that the LGM PMIP4-CMIP6 simulations are less cold. As a result, net precipitation (precipitation minus evapotranspiration) in the PMIP4-CMIP6 ensemble is higher at the LGM than the PI in the extratropics—particularly over the mid-latitude eastern Pacific in

280   both hemispheres and over most of North America—with the exception of the North Atlantic where evaporation decreases are more localized and do not compensate for the reductions in precipitation (Fig. 8, right). This, together with colder temperatures, could help explain why the PMIP4-CMIP6 models simulate a stronger AMOC at the LGM. Substantial reductions in continental net precipitation only occur over tropical South America and high-latitude regions, while Africa, Australia, and the mid-latitude regions of Eurasia and the Americas see little change or even increased net precipitation.

285

4 Data-model comparisons

The evaluation of the PMIP3-CMIP5 LGM simulations showed that large scale climate features, such as the ratio of changes in land-sea temperature, in high-latitude temperature amplification, and in precipitation scaling with temperature were broadly consistent with modern observations (Braconnot et al., 2012; Izumi et al., 2013; Harrison et al., 2014, 2015).

290

The ratio for the land-sea difference in changes in mean annual temperature in the tropics in the PMIP4-CMIP6 simulations is compatible with the ratio reconstructed from the Bartlein et al. (2011) and MARGO (2009) data sets. However, the simulated ocean temperatures in the PMIP3-CMIP5 simulations are somewhat too cold compared to the MARGO (2009) reconstructions. Although the Cleator et al. (2019) data set has a larger spatial coverage than the Bartlein et al. (2011) data set, there is no

295 significant difference between the two data sets for most of the temperature variables across common grid cells (Fig 9). However, the new reconstructions have a reduced range at the warm end so that some simulations are recorded as warmer than the land-based reconstructions (Fig. 10). The reconstructions of the LGM - Late Holocene SST anomalies provided by Tierney et al (2019) are colder than the MARGO reconstructions in the tropics and, although this removes the apparent cold-bias shown by some simulations, this results in some simulations falling outside the window of reconstructed SSTs at the warm

300 end. Overall, the comparison with the new data sets suggests that both ensembles produce changes in tropical land-sea contrast that are realistic, though slightly too warm over both land and ocean. At the global scale (Fig. 10, right), the new SST reconstructions indicate colder ocean temperatures than the MARGO (2009) data set, whereas the land-based reconstructions of Cleator et al. (2019) show somewhat warmer temperatures than the Bartlein et al (2011) data set. As a result of these changes, and the increased variability simulated in extratropical regions, there are larger discrepancies between the simulated

305 and reconstructed land-sea contrast, with some models showing too cold conditions, while other models show too warm conditions over both land and ocean. However, the match between the simulations and the new reconstructions overall is better than the match with the Bartlein et al. (2011) and MARGO (2009) reconstructions.

The amplification of temperature changes at high northern latitudes compared to the tropics is apparent over both the land and

310 the ocean domains, although the amplification appears to be smaller in the new data syntheses (Fig. 11). For the ocean domain, this could reflect the influence of seasonal production on the extratropical sites, with indicators being more sensitive to summer changes, or to changes in the seasonal production cycle. Comparisons of the amplification over land areas with the Bartlein et al. (2011) data set suggest that the simulated tropical cooling is too large in the PMIP3-CMIP5 simulations whereas the extratropical cooling was both larger and smaller than suggested by the reconstructions in both ensembles. Simulated tropical

315 temperatures are more consistent with the Cleator et al. (2019) reconstructions, suggesting that the apparent over-estimation of tropical cooling in the PMIP3-CMIP5 simulations over land may reflect the paucity of tropical data points in Bartlein et al (2011). However, the discrepancies between the simulated and reconstructed extratropical land temperatures are still present:

Climate
of the Past
Discussions

Open Access

EGU

there are several PMIP3-CMIP5 simulations that are much colder than the reconstructions, whereas the currently available PMIP4-CMIP6 simulations tend to be warmer than the reconstructions. Although polar amplification is more muted over the
320   ocean domain, the comparisons show a similar picture to the land-based comparisons. Simulated tropical ocean temperatures are more compatible with the Tierney et al. (2019) than the MARGO (2009) synthesis. Simulated extratropical temperature changes in the PMIP3-CMIP5 ensemble are considerably colder than shown by either of these syntheses. However, whereas none of the models showed the warmer conditions implied by the MARGO (2009) compilation, two models (iLOVECLIM from PMIP4-CMIP6, CRNM-CM5 from PMIP3-CMIP5) show slightly warmer extratropical temperatures than indicated by
325   Tierney et al. (2019).

The LGM climate is characterised by an increase in temperature seasonality in extratropical regions, with larger changes in winter than in summer (Izumi et al., 2013). In general, this change in seasonality is reproduced by the models. However, the simulated change in winter temperature is smaller than indicated by the reconstructions (Fig. 12, top line). The magnitude of
330   the summer cooling is more consistent in the PMIP4-CMIP6 simulations than in the PMIP3-CMIP5 simulations in North America, Europe and Eurasia. Simulated changes in summer temperature are more consistent with the reconstructions than simulated changes in winter temperature. Although the PMIP3-CMIP5 simulated winter temperatures over North America are broadly consistent with the reconstructions, the PMIP4-CMIP6 simulations are generally warmer than the reconstructed temperatures. Simulated winter temperatures in Europe are generally outside the range of the reconstructions for both
335   ensembles. This is consistent with the fact that the simulated SSTs in the North Atlantic are generally warmer than the reconstructions, given that the mean annual temperature signal (over land and ocean) is dominated by changes in the winter temperature. Over extratropical Eurasia, the PMIP3-CMIP5 models simulate an amplification of the seasonal cycle, but overestimate both the winter and summer cooling compared to the Cleator et al. (2019) reconstructions, which are much warmer than the Bartlein et al. (2011) reconstructions. The PMIP4-CMIP6 models are more consistent with the reconstructions,
340   with 4 simulations (AWIESM1 and 2 and both iLOVECLIM1.4) being within the range of uncertainty for both winter and summer temperature. Other PMIP4-CMIP6 models overestimate the cooling in both seasons, but less so than the PMIP3-CMIP5 models. This could reflect the lower climate sensitivities of the currently available PMIP4-CMIP6 compared to the PMIP3-CMIP5 models, or the changes in the ice-sheet altitude and their impact on planetary waves.

345   Regional changes in the tropics (Fig. 12, bottom line) are more muted than those in the northern extratropics, and seasonality differences are small. We therefore base our comparisons on the mean annual temperature (MAT) and mean annual precipitation (MAP). The PMIP3-CMIP5 models simulate MAT consistent with both data syntheses over tropical America and Africa and with the Bartlein et al. (2011) simulation over Asia, while PMIP4-CMIP6 models underestimate tropical cooling -- most noticeably in tropical America. This is probably related to the simulated tropical SSTs being warmer than the
350   Tierney et al. (2019) reconstructions. The reconstructed changes in tropical precipitation are generally small (Fig. 12), except in the case of tropical Africa where there is a large difference between the Bartlein et al. (2011) and the Cleator et al. (2019)

Climate
of the Past
Discussions

reconstructions. Although there is considerable within-model variability, the PMIP3-CMIP5 and PMIP4-CMIP6 simulations are consistent with the precipitation reconstructions for the Americas and Asia, with only a few models simulating conditions too dry compared to the reconstructions. Although both the PMIP3-CMIP5 and PMIP4-CMIP6 ensembles produce a cooling

355   in Africa consistent with the reconstructions, simulated changes in precipitation are generally smaller than indicated by observations. There is, however, a large difference between the estimates of precipitation change given by the Bartlein et al. (2011) and the Cleator et al. (2019) data sets for tropical Africa, and the simulated changes in precipitation are more consistent with the newer data set. The PMIP4-CMIP6 models are more consistent with the temperature reconstructions over tropical Asia, but show poorer agreement with the precipitation reconstructions than the PMIP3-CMIP5 models. There is no systematic

360   improvement in the simulation of tropical climates between the PMIP4-CMIP6 and PMIP3-CMIP5 ensembles. The biases are different, with some regions/variables better represented by the PMIP3-CMIP5 models (e.g. tropical Americas and Africa for the temperatures, tropical Asia for precipitation), while others are better represented by the PMIP4-CMIP6 models (tropical Americas for precipitation, tropical Asia for temperatures).

365   The four data syntheses can be used together to constrain the global MAT change from LGM to PI. There is a good correlation between the change in global average MAT over the reconstruction grid points and computed taking all the model grid points into account (Fig. 13). There are models with results below, within and above the average of all of the reconstructions except MARGO (2009) where there is no model with MAT above the reconstructed value. Retaining only the models which produce changes in MAT consistent with the reconstructions (and reconstruction uncertainty), the globally averaged change in MAT

370   is between -5.3 and -3.7°C using the Bartlein et al. (2011) and the Cleator et al. (2019) data sets, between -4.9 and -3.2°C for the Tierney et al. (2019) data set and above -3.9°C for the MARGO (2009) data set. These estimates are slightly warmer than previous estimates, which indicate changes in MAT of between 4 and 6°C (Annan and Hargreaves, 2015; Friedrich et al., 2016).

375   **5 Conclusions and perspectives**

The results from the PMIP4-CMIP6 models differ from those of the PMIP3-CMIP5 in several ways. The amplitude of the global and large-scale cooling is smaller in the PMIP4-CMIP6 ensemble, which is probably a result of the weaker climate sensitivity of the current ensemble and the lower altitude of the ice sheets prescribed as boundary conditions.. This change in the ice sheets also has an impact on atmospheric circulation over North America and the North Atlantic, but possibly over

380   extratropical Eurasia too. The AMOC increases less in the PMIP4-CMIP6 than in the PMIP3-CMIP5 simulations, and the depth of the NADW cell remains stable, in contrast with half the models of the PMIP3-CMIP5 ensemble, which simulated a large deepening of this cell. This could be due to the changes in atmospheric circulation over the North Atlantic, as well as changes in the North Atlantic freshwater balance. Changes in precipitation are generally similar for the PMIP3-CMIP5 and PMIP4-CMIP6 ensembles and characterised by less precipitation overall. Reduced evaporation due to colder temperatures

385   partially compensates for the reduction in precipitation, so that areas of positive LGM - PI anomalies in net precipitation (i.e. precipitation minus evaporation) are larger than areas with positive LGM - PI precipitation anomalies. However, both precipitation and net precipitation changes show large spatial heterogeneity, and different regional-scale patterns of change between the PMIP4-CMIP6 and PMIP3-CMIP5 ensembles, which could be related to the difference in atmospheric circulation and temperature changes. Additional sensitivity experiments are needed to separate the effects of changes in model

390   configuration and sensitivity on general circulation features, such as the position of the jet streams, from the effects of differences in boundary conditions, such as the improved realism of the ice sheet configuration.

The PMIP4-CMIP6 ensemble confirms that the models capture large-scale thermodynamic behaviour, such as land-sea contrast and polar amplification, well. Indeed, the match of both the PMIP3-CMIP5 and PMIP4-CMIP6 results to the new

395   reconstructions of Tierney et al. (2019) and Cleator et al. (2019) is better than with the reconstructions used to evaluate these features previously (Braconnot et al., 2012; Izumi et al., 2013; Harrison et al., 2014, 2015). The simulated global change in MAT averaged over all the grid cells where reconstructions are available is well correlated with the global average on all model grid points, providing a constraint on the value of the global LGM cooling compared to PI. Using the terrestrial data sets as a constraint, indicates a global cooling between -5.3 and -3.7°C, while using Tierney et al. (2019) as a constraint

400   indicates a global cooling of -4.9 to -3.2°C. The MARGO (2009) data set does not provide a strong constraint on the upper limit of the cooling because no model simulates warmer temperature anomalies than these reconstructions. The constrained range (-5.3 to -3.2°C) is less extreme than previous estimates(-4 to -6°C).

There is no obvious improvement in model performance at a regional scale between the PMIP3-CMIP5 and PMIP4-CMIP6

405   ensembles. In some cases (e.g mean annual temperature change over the tropical Americas), the PMIP3-CMIP5 ensemble demonstrate a better ability to capture the changes depicted by the reconstructions, in some other (e.g. winter and summer temperatures over extratropical Asia, summer temperatures over North America, winter temperatures over Europe), the PMIP4-CMIP6 ensemble is clearly better.

410   Our analyses present a first picture of the PMIP4-CMIP6 LGM experiments. Results from CMIP6 models with high climate sensitivity are not available yet, but will need to be considered in a full assessment of the PMIP4-CMIP6 simulations. Sensitivity experiments, for example to different ice sheet configurations, are needed to disentangle the impact of model improvements from those related to using more realistic boundary conditions. Additional planned simulations will also help to disentangle the impacts of changes in vegetation and aerosol loading on the LGM climate. A more systematic evaluation of

415   the simulated climates, using a wider range of palaeoenvironmental data, will be helpful in understanding why there are persistent mismatches between the simulations and reconstructions at a regional scale. Nevertheless, this preliminary analysis demonstrates the utility of the PMIP4-CMIP6 simulations in addressing questions about the response of climate to large changes in forcing and illustrates the need to investigate the causes of inter-model differences in these responses.

Climate
of the Past
Discussions

430

References

Abe-Ouchi, A., Saito, F., Kageyama, M., Braconnot, P., Harrison, S. P., Lambeck, K., Otto-Bliesner, B. L., Peltier, W. R., Tarasov, L., Peterschmitt, J.-Y., and Takahashi, K.: Ice-sheet configuration in the CMIP5/PMIP3 Last Glacial Maximum

435 experiments, Geosci. Model Dev., 8, 3621–3637, https://doi.org/10.5194/gmd-8-3621-2015, 2015.

Adloff, M., Reick, C. H., and Claussen, M.: Earth system model simulations show different feedback strengths of the terrestrial carbon cycle under glacial and interglacial conditions, Earth Syst. Dynam., 9, 413–425, https://doi.org/10.5194/esd-9-413-2018, 2018.

440

Annan, J. D. and Hargreaves, J. C.: A perspective on model-data surface temperature comparison at the Last Glacial Maximum, Quaternary Science Reviews, 107, 1-10, https://doi.org/10.1016/j.quascirev.2014.09.019, 2015.

Argus, D. F., Peltier, W. R., Drummond, R., and Moore, A. W.: The Antarctica component of postglacial rebound model ICE-

445 6G_C(VM5a) based on GPS positioning, exposure age dating of ice thicknesses, and relative sea level histories, Geophys. J. Int., 198,537–563, doi:10.1093/gji/ggu140, 2014.

Bartlein, P. J., Harrison, S.P., Brewer, S., Connor, S., Davis B.A.S., Gajewski, K., Guiot, J., Harrison-Prentice, T.I., Henderson, A., Peyron, O., Prentice, I.C., Scholze, M., Seppä, H., Shuman, B., Sugita, S., Thompson, R.S., Viau, A., Williams, J., Wu, H.,: Pollen-based continental climate reconstructions at 6 and 21 ka: a global synthesis, Climate Dynamics 37, 775-802, 2011.

Beghin, P., Charbit, S., Dumas, C., Kageyama, M., and Ritz, C.: How might the North American ice sheet influence the northwestern Eurasian climate?, Clim. Past, 11, 1467–1490, https://doi.org/10.5194/cp-11-1467-2015, 2015.

Beghin, P., Charbit, S., Kageyama, M., Combourieu Nebout, N., Hatté, C., Dumas, C., and Peterschmitt, J.-Y.: What drives LGM precipitation over the western Mediterranean? A study focused on the Iberian Peninsula and northern Morocco, Climate Dynamics, 46, 2611-2631, 2016.

Böhm, E., Lippold, J., Gutjahr, M., Frank, M., Blaser, P., Antz, B., Fohlmeister, J., Frank, N., Andersen, M., B., and Deininger, M.: Strong and deep Atlantic meridional overturning circulation during the last glacial cycle, Nature, 517, 73-76, doi:10.1038/nature14059, 2015.

Boos, W. R.: Thermodynamic Scaling of the Hydrological Cycle of the Last Glacial Maximum. Journal of Climate, 25, 992-,1006, https://doi.org/10.1175/JCLI-D-11-00010.1, 2012.

Braconnot, P., Harrison, S. P., Kageyama, M., Bartlein, P. J., Masson-Delmotte, V., Abe-Ouchi, A., Otto-Bliesner, B., and Zhao, Y.: Evaluation of climate models using palaeoclimatic data, Nature Climate Change, 2, 417-424, 2012.

Brady, E. C., Otto-Bliesner, B. L., Kay, J. E. and Rosenbloom, N.: Sensitivity to Glacial Forcing in the CCSM4, J. Clim., 26, 1901-1925, doi: 10.1175/JCLI-D-11-00416.1, 2013.

Bragg, F. J., Prentice, I. C., Harrison, S. P., Eglinton, G., Foster, P. N., Rommerskirchen, F., and Rullkötter, J.: Stable isotope and modelling evidence for CO_2 as a driver of glacial–interglacial vegetation shifts in southern Africa, Biogeosciences, 10, 2001–2010, https://doi.org/10.5194/bg-10-2001-2013, 2013.

Chandan, D. and Peltier, W. R.: Regional and global climate for the mid-Pliocene using the University of Toronto version of CCSM4 and PlioMIP2 boundary conditions, Clim. Past, 13, 919–942, https://doi.org/10.5194/cp-13-919-2017, 2017.

Climate
of the Past
Discussions

Chandan, D. and Peltier, W. R.: On the mechanisms of warming the mid-Pliocene and the inference of a hierarchy of climate sensitivities with relevance to the understanding of climate futures, Clim. Past, 14, 825–856, https://doi.org/10.5194/cp-14-825-2018, 2018.

Cleator, S. F., Harrison, S. P., Nichols, N. K., Prentice, I. C., and Roulstone, I.: A new multi-variable benchmark for Last Glacial Maximum climate simulations, Clim. Past Discuss., https://doi.org/10.5194/cp-2019-55, in review, 2019.

Crowley, T. J.: CLIMAP SSTs re-revisited, Clim. Dynamics 16(4): 241-255, 2000

DiNezio, P. and Tierney, J. E.: The effect of sea level on glacial Indo-Pacific climate, Nat. Geoscience, 6, 485–491. doi: 10.1038/ngeo1823, 2013.

Galbraith, E. and de Lavergne, C.: Response of a comprehensive climate model to a broad range of external forcings: relevance for deep ocean ventilation and the development of late Cenozoic ice ages. Climate Dynamics, 52: 653. https://doi.org/10.1007/s00382-018-4157-8, 2019.

Gerhart, L. M. & Ward, J. K.: Plant responses to low [CO2] of the past. *New Phytologist* **188,** 674–695, 2010.

Goldsmith, Y.. Polissar, P., Ayalon, A., Bar-Matthews, M., Demenocal, P., Broecker, W.S.: The modern and Last Glacial Maximum hydrological cycles of the Eastern Mediterranean and the Levant from a water isotope perspective. Earth and Planetary Science Letters 457: 0.1016/j.epsl.2016.10.017, 2017.

Hajima, T., Watanabe, M., Yamamoto, A., Tatebe, H., Noguchi, M. A., Abe, M., Ohgaito, R., Ito, A., Yamazaki, D., Okajima, H., Ito, A., Takata, K., Ogochi, K., Watanabe, S., and Kawamiya, M.: Description of the MIROC-ES2L Earth system model and evaluation of its climate–biogeochemical processes and feedbacks, Geosci. Model Dev. Discuss., https://doi.org/10.5194/gmd-2019-275, in review, 2019.

Harrison, S. P., Bartlein, P. J., Brewer, S., Prentice, I. C., Boyd, M., Hessler, I., Holmgren, K., Izumi, K., and Willis, K.: Climate model benchmarking with glacial and mid-Holocene climates, Climate Dynamics 43, 671-688, 2014.

Harrison, S. P., Bartlein, P. J., Izumi, K., Li, G., Annan, J., Hargreaves, J., Braconnot, P., and Kageyama, M.: Evaluation of CMIP5 palaeo-simulations to improve climate projections, Nature Clim. Change 5, 735-743, doi:10.1038/nclimate2649, 2015.

Ivanovic, R. F., Gregoire, L. J., Kageyama, M., Roche, D. M., Valdes, P. J., Burke, A., Drummond, R., Peltier, W. R., and Tarasov, L.: Transient climate simulations of the deglaciation 21–9 thousand years before present (version 1) – PMIP4 Core experiment design and boundary conditions, Geosci. Model Dev., 9, 2563–2587, https://doi.org/10.5194/gmd-9-2563-2016, 2016.

Hu, A., X., Meehl, G., A., Han, W., Q., Otto-Bliestner, B., Abe-Ouchi, A., and Rosenbloom, N.: Effects of the Bering Strait closure on AMOC and global climate under different background climates. Prog Oceanography, 132:174–196. doi:10.1016/j.pocean.2014.02.004, 2015.

510

Izumi, K., Bartlein, P. J., and Harrison, S. P.: Consistent large-scale temperature responses in warm and cold climates, Geophys. Res. Lett., 40, 1817–1823, doi:10.1002/grl.50350, 2013.

Kageyama, M., Albani, S., Braconnot, P., Harrison, S. P., Hopcroft, P. O., Ivanovic, R. F., Lambert, F., Marti, O., Peltier, W.
515   R., Peterschmitt, J.-Y., Roche, D. M., Tarasov, L., Zhang, X., Brady, E. C., Haywood, A. M., LeGrande, A. N., Lunt, D. J., Mahowald, N. M., Mikolajewicz, U., Nisancioglu, K. H., Otto-Bliesner, B. L., Renssen, H., Tomas, R. A., Zhang, Q., Abe-Ouchi, A., Bartlein, P. J., Cao, J., Li, Q., Lohmann, G., Ohgaito, R., Shi, X., Volodin, E., Yoshida, K., Zhang, X., and Zheng, W.: The PMIP4 contribution to CMIP6 – Part 4: Scientific objectives and experimental design of the PMIP4-CMIP6 Last Glacial Maximum experiments and PMIP4 sensitivity experiments, Geosci. Model Dev., 10, 4035–4055,
520   https://doi.org/10.5194/gmd-10-4035-2017, 2017.

Kageyama, M., Braconnot, P., Harrison, S. P., Haywood, A. M., Jungclaus, J. H., Otto-Bliesner, B. L., Peterschmitt, J.-Y., Abe-Ouchi, A., Albani, S., Bartlein, P. J., Brierley, C., Crucifix, M., Dolan, A., Fernandez-Donado, L., Fischer, H., Hopcroft, P. O., Ivanovic, R. F., Lambert, F., Lunt, D. J., Mahowald, N. M., Peltier, W. R., Phipps, S. J., Roche, D. M., Schmidt, G. A.,
525   Tarasov, L., Valdes, P. J., Zhang, Q., and Zhou, T.: The PMIP4 contribution to CMIP6 – Part 1: Overview and over-arching analysis plan, Geosci. Model Dev., 11, 1033–1057, https://doi.org/10.5194/gmd-11-1033-2018, 2018.

Kirby, M. E., Feakins, S. J., Bonuso, N., Fantozzi, J. M. and Hiner, C. A.: Latest Pleistocene to Holocene hydroclimates from Lake Elsinore, California, Quat. Sci. Rev., 76, 1–15. http://dx.doi.org/10.1016/j.quascirev.2013.05.023, 2013.

530

Klockmann, M., Mikolajewicz, U., & Marotzke, J.: The effect of greenhouse gas concentrations and ice sheets on the glacial AMOC in a coupled climate model. Climate of the Past, 1829–1846. https://doi.org/10.5194/cp-12-1829-2016, 2016.

Laîné, A., M. Kageyama, D. Salas-Mélia, A. Voldoire, G. Rivière, G. Ramstein, S. Planton, S. Tyteca, J.Y. Peterschmitt:
535   Northern hemisphere storm tracks during the Last Glacial Maximum in the PMIP2 Ocean-Atmosphere coupled models: energetic study, seasonal cycle, precipitation, Climate Dynamics, 32, 593-614. DOI: 10.1007/s00382-008-0391-9, 2009.

Li, G., Harrison, S.P., Bartlein, P.J., Izumi, K., Prentice, I.C.:Precipitation scaling with temperature in warm and cold climates: an analysis of CMIP5 simulations. *Geophysical Research Letters* 40:4018-4024, doi:10.1002/grl.50730, 2013.

540

Liakka, J. and Lofverstrom, M.: Arctic warming induced by the Laurentide Ice Sheet topography, Clim. Past, 14, 887–900, https://doi.org/10.5194/cp-14-887-2018, 2018.

Lofverstrom, M: A dynamic link between high-intensity precipitation events in southwestern North America and Europe at the Last Glacial Maximum, in review in EPSL

Lofverstrom, M, Caballero, R., Nilsson, J., Kleman, J.: Evolution of the large-scale atmospheric circulation in response to changing ice sheets over the last glacial cycle, Climate of the Past, 10, 1453-1471, https://doi.org/10.5194/cp-10-1453-2014, 2014.

Lofverstrom, M, Caballero, R., Nilsson, J., Messori, G.: Stationary Wave Reflection as a Mechanism for Zonalizing the Atlantic Winter Jet at the LGM, Journal of the Atmospheric Sciences, 73, 3329-3342, https://doi.org/10.1175/JAS-D-15-0295.1, 2016.

Lofverstrom, M., and Lora, J. M., Abrupt regime shifts in the North Atlantic atmospheric circulation over the last deglaciation, *Geophys. Res. Lett.*, 44, 8047– 8055, doi:10.1002/2017GL074274, 2017.

Lora, J. M., J. L. Mitchell, C. Risi, and Tripati,A. E. North Pacific atmo- spheric rivers and their influence on western North America at the Last Glacial Maximum. Geophys. Res. Lett., 44, 1051–1059, https://doi.org/10.1002/2016GL071541, 2017.

Lora, J. M.: Components and Mechanisms of Hydrologic Cycle Changes over North America at the Last Glacial Maximum, Journal of Climate, 31, 7035-7051, https://doi.org/10.1175/JCLI-D-17-0544.1, 2018.

Lynch-Stieglitz, J., Adkins, J. F., Curry, W. B., Dokken, T., Hall, I. R., Herguera, J. C., Hirschi, J. J.-M., Ivanova, E. V., Kissel, C., Marchal, O., Marchitto, T. M., McCave, I. N., McManus, J. F., Mulitza, S., Ninnemann, U., Peeters, F., Yu, E.-F., and Zahn, R.: Atlantic Meridional Overturning Circulation During the Last Glacial Maximum, Science, 316, 66, DOI: 10.1126/science.1137127, 2007.

Malevich, S. B., Vetter, L., and Tierney, J. E.: Global core top calibration of δ18O in planktic foraminifera to sea surface temperature, Paleoceanography and Paleoclimatology, 34, 1292–1315, 2019.

MARGO Project Members: Constraints on the magnitude and patterns of ocean cooling at the Last Glacial Maximum, Nature Geosci., 2, 127-132, 2009.

575   Masson-Delmotte, V., Dreyfus, G., Braconnot, P., Johnsen, S., Jouzel, J., Kageyama, M., Landais, A., Loutre, M.-F., Nouet, J., Parrenin, F., Raynaud, D., Stenni, B., and Tuenter, E.: Past temperature reconstructions from deep ice cores: relevance for future climate change, Clim. Past, 2, 145–165, https://doi.org/10.5194/cp-2-145-2006, 2006.

       Mauritsen, T.,et al.: Developments in the MPI-M Earth System Model version 1.2 (MPI-ESM1.2) and its response to
580   increasing CO2. Journal of Advances in Modeling Earth Systems, 11, 998–1038. https://doi.org/10.1029/2018MS001400, 2019.

       Mix, A. C., Morey, A. E., Pisias, N. G., & Hostetler, S. W.: Foraminiferal faunal estimates of paleotemperature: Circumventing the no-analog problem yields cool ice age tropics. Paleoceanography, 14(3), 350-359, 1999.

585

       Morrill, C., Lowry, D. P. and Hoell, A.: Thermodynamic and dynamic causes of pluvial conditions during the Last Glacial Maximum in western North America. Geophys. Res. Lett. 45, 335–345, 2018.

       Muglia, J., and Schmittner, A.: Glacial Atlantic overturning increased by wind stress in climate models, Geophys. Res. Lett.,
590   42, 9862–9869, doi:10.1002/2015GL064583, 2015.

       Oka, A., Hasumi, H., and Abe-Ouchi, A.: The thermal threshold of the Atlantic meridional overturning circulation and its control by wind stress forcing during glacial climate. Geophysical Research Letters, 39, L09709. doi:10.1029/2007gl029475, 2012.

595

       Peltier, W. R., Argus, D. F., and Drummond, R.: Space geodesy constrains ice age terminal deglaciation: The global ICE-6G_C(VM5a) model, J. Geophys. Res.-Sol. Ea., 120, 450–487,doi:10.1002/2014JB011176, 2015.

       Prentice, I.C. and Harrison, S.P.: Ecosystem effects of CO_2 concentration: evidence from past climates. *Climates of the Past*
600   5: 297-307, 2009.

       Prentice, I.C., Cleator, S.F., Huang, Y.F., Harrison, S.P., and Roulstone, I.: Reconstructing ice –age climates: quantifying low-CO_2 effects on plants. *Global and Planetary Change* 149: 166-176. http://dx.doi.org/10.1016/j.gloplacha.2016.12.012, 2017.

605

Scheff, J., and Frierson, D. M. W.: Robust future precipitation declines in CMIP5 largely reflect the poleward expansion of model subtrop-ical dry zones, Geophys. Res. Lett., 39, L18704, doi:10.1029/2012GL052910, 2012.

610 Scheff, J., Seager, R. and Liu, H.: Are glacials dry? Consequences for paleoclimatology and for greenhouse warming. J. Climate, 30, 6593–6609, https://doi.org/10.1175/JCLI-D-16-0854.1, 2017.

Schmidt, G. A., Annan, J. D., Bartlein, P. J., Cook, B. I., Guilyardi, E., Hargreaves, J. C., Harrison, S. P., Kageyama, M., LeGrande, A. N., Konecky, B., Lovejoy, S., Mann, M. E., Masson-Delmotte, V., Risi, C., Thompson, D., Timmermann, A., Tremblay, L.-B., and Yiou, P.: Using palaeo-climate comparisons to constrain future projections in CMIP5, Clim. Past, 10,

615 221–250, https://doi.org/10.5194/cp-10-221-2014, 2014.

Sherriff-Tadano, S. and Abe-Ouchi, A.: Roles of sea ice–surface wind feedback in maintaining the glacial Atlantic meridional overturning circulation and climate. Journal of Climate. https://doi.org/10.1175/JCLI-D-19-0431.1, 2020.

620 Sherriff-Tadano, S., Abe-Ouchi, A., Yoshimori, M., Oka, A., and Chan, W.-L.: Influence of glacial ice sheets on the Atlantic meridional overturning circulation through surface wind change. Climate Dynamics, 50, 2881-2903. doi: 10.1007/s00382-017-3780-0, 2018.

Sidorenko, D. , Rackow, T. , Jung, T. , Semmler, T. , Barbi, D. , Danilov, S. , Dethloff, K. , Dorn, W. , Fieg, K. , Gößling, H.

625 F. , Handorf, D. , Harig, S. , Hiller, W. , Juricke, S. , Losch, M. , Schröter, J. , Sein, D. and Wang, Q.: Towards multi-resolution global climate modeling with ECHAM6–FESOM. Part I: model formulation and mean climate, Climate Dynamics, 44, 757-780 . doi: 10.1007/s00382-014-2290-6, 2015.

Sidorenko, D., H. F. Goessling, N. Koldunov, P. Scholz, S. Danilov, D. Barbi, W. Cabos, O. Gurses, S. Harig, C. Hinrichs, S.

630 Juricke, G. Lohmann, M. Losch, L. Mu, T. Rackow, N. Rakowsky, D. Sein, T. Semmler, X. Shi, C. Stepanek, J. Streffing, Q. Wang, C. Wekerle, H. Yang, T. Jung: Evaluation of FESOM2.0 coupled to ECHAM6.3: Pre-industrial and HighResMIP simulations. Journal of Advances in Modeling Earth Systems, 11, DOI: 10.1029/2019MS001696, 2019.

Sueyoshi, T., Ohgaito, R., Yamamoto, A., Chikamoto, M. O., Hajima, T., Okajima, H., Yoshimori, M., Abe, M., O'ishi, R.,

635 Saito, F., Watanabe, S., Kawamiya, M., and Abe-Ouchi, A.: Set-up of the PMIP3 paleoclimate experiments conducted using an Earth system model, MIROC-ESM, Geosci. Model Dev., 6, 819–836, https://doi.org/10.5194/gmd-6-819-2013, 2013.

Telford, R. J., Li, C., and Kucera, M.: Mismatch between the depth habitat of planktonic foraminifera and the calibration depth of SST transfer functions may bias reconstructions. Climate of the Past, 9(2), 859-870, 2013.

640

Tierney, J. E., and Tingley, M. P.: A TEX 86 surface sediment database and extended Bayesian calibration. Scientific data, 2, 150029, 2015.

Tierney, J. E., and Tingley, M. P.: BAYSPLINE: A new calibration for the alkenone paleothermometer. Paleoceanography
645   and Paleoclimatology, 33(3), 281-301, 2018.

Tierney, J. E., Malevich, S. B., Gray, W., Vetter, L., and Thirumalai, K. : Bayesian calibration of the Mg/Ca paleothermometer in planktic foraminifera. Paleoceanography and Paleoclimatology; 2019.

650   Tierney, J. E., Zhu, J., King, J., Malevich, S. B., Hakim, G., & Poulsen, C.: Glacial cooling and climate sensitivity revisited. https://doi.org/10.31223/osf.io/me5uj, December 26, 2019.

Ullman, D. J., LeGrande, A. N., Carlson, A. E., Anslow, F. S., and Licciardi, J. M.: Assessing the impact of Laurentide Ice Sheet topography on glacial climate, Clim. Past, 10, 487–507, https://doi.org/10.5194/cp-10-487-2014, 2014.
655

Voldoire, A., Sanchez-Gomez, E., Salas y Mélia, D., Decharme, B., Cassou, C., Sénési, S., Valcke, S., Beau, I., Alias, A. Chevallier, M., Déqué, M., Deshayes, J., Douville, H., Fernandez, E., Madec, G., Maisonnave , E., Moine, M.-P., Planton, S., Saint-Martin, D., Szopa, S., Tyteca, S., Alkama, R., Belamari, S., Braun, A., Coquart, L. and Chauvin., F. : The CNRM-CM5.1 global climate model : description and basic evaluation, Climate Dynamics, 40, 2091-2121, DOI:10.1007/s00382-011-1259-
660   y, 2013.

Zhang, X., Lohmann, G., Knorr, G. and Purcell, C.: Abrupt glacial climate shifts controlled by ice sheet changes. Nature 512:290– 294. doi:10.1038/nature13592, 2014.

665 **Table 1: PMIP3 and PMIP4 models analysed in the present study. The spin-up duration is only given for the new PMIP4-CMIP6 simulations.**

Model	Climate sensitivity ΔT^{eq}	Reference	Ice sheets	Spin-up duration (years)	PMIP/CMIP phase and rip(f)	Additional comments
CCSM4	2.9	Brady et al., 2013	PMIP3		PMIP3-CMIP5 r1i1p1	
CNRM-CM5	3.3	Voldoire et al., 2013	PMIP3		PMIP3-CMIP5 r1i1p1	
GISS-E2-R	2.1	Ullman et al. 2014	PMIP3		PMIP3-CMIP5 r1i1p150	PMIP3 ice sheet
GISS-E2-R	2.1	Ullman et al. 2014	PMIP3		PMIP3-CMIP5 r1i1p151	ICE-5G ice extent but lower Laurentide Ice Sheet altitude
IPSL-CM5A-LR	4.1	Dufresne et al., 2013	PMIP3		PMIP3-CMIP5 r1i1p1	
MIROC-ESM	4.7	Sueyoshi et al. 2013	PMIP3		PMIP3-CMIP5 r1i1p1	initial ocean state was taken from PMIP2 MIROC4m
MPI-ESM-P	3.5		PMIP3		PMIP3-CMIP5 r1i1p1	AO, initial state for spin-up from PMIP2 simulation
MPI-ESM-P	3.5	Adloff et al., 2018	PMIP3		PMIP3-CMIP5 r1i1p2	AOV
MRI-CGCM3	2.6		PMIP3		PMIP3-CMIP5 r1i1p1	
AWIESM1	3.6	Sidorenko et al., 2015	ICE-6G_C	1200	PMIP4-CMIP6	
AWIESM2	3.6	Sidorenko et al., 2019	ICE-6G_C	1200	PMIP4-CMIP6	

UoT-CCSM4	3.2	Chandan and Peltier, 2018, Chandan and Peltier, 2017	ICE-6G_C	2900 years	PMIP4-CMIP6	
iLOVECLIM1.1.4	3.2 (after 2500 years)		GLAC-1D	5000	PMIP4-CMIP6	5000 years from a PI restart; EMIC
iLOVECLIM1.1.4	3.2 (after 2500 years)		ICE-6G_C	5000	PMIP4-CMIP6	5000 years from a PI restart; EMIC
MIROC-ES2L	2.7	Hajima et al. GMDD	ICE-6G_C	8960	PMIP4-CMIP6 r1i1p1f2	First 6760 years integrated using the MIROC-ES2L physical core; followed by 2200 years integrated using the full MIROC-ES2L ESM.
MPI-ESM1.2	2.77	Mauritsen et al., 2019	ICE-6G_c	3850	PMIP4-CMIP6 r1i1p1f1	3850 years after restart from a previous lgm simulation.
INM-CM4-8	2.1	Volodin et al., 2018	ICE-6G_C	50	PMIP4-CMIP6 r1i1p1f1	

670
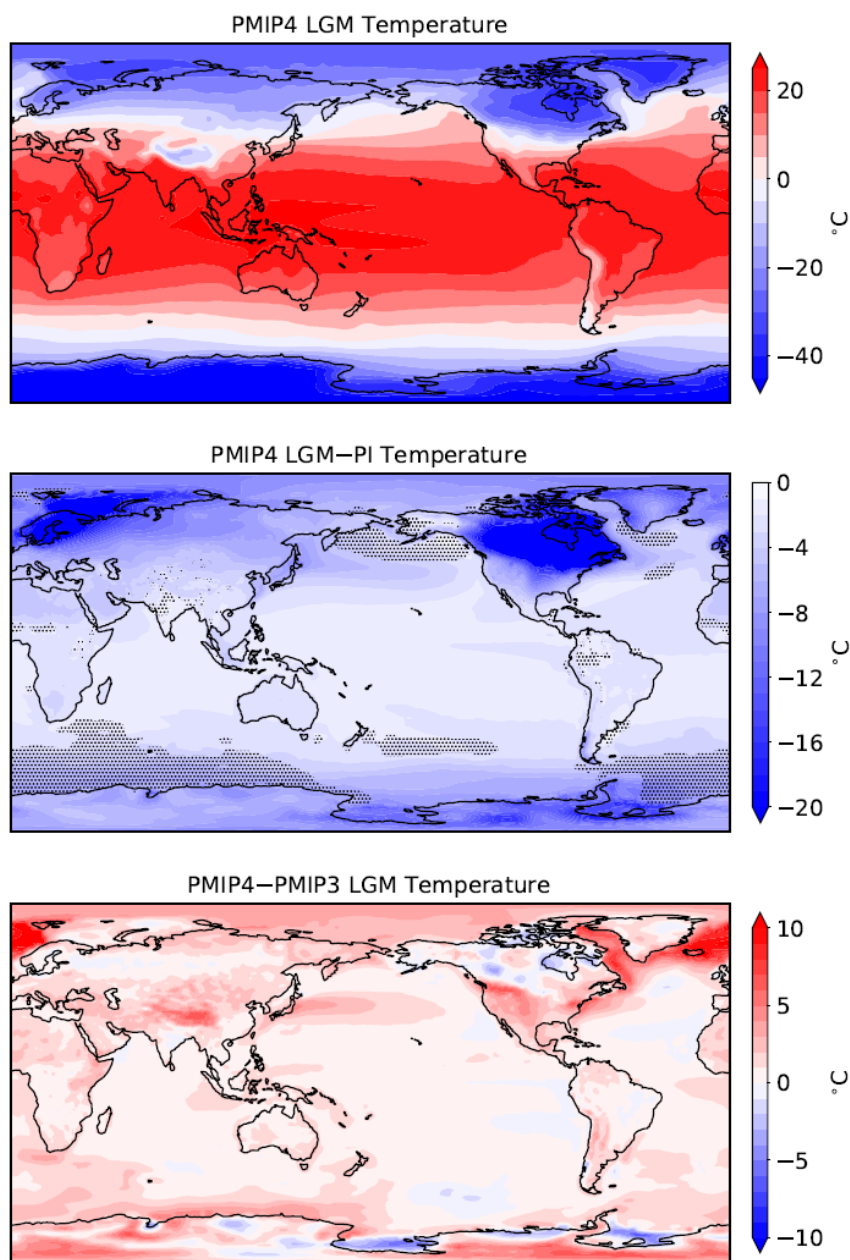
Figure 1: LGM mean annual temperature (in °C) simulated by the ensemble of PMIP4 models (top), LGM – PI mean annual temperature anomaly (in °C) simulated by the same models (middle, where stippling shows where models do not agree on the sign of changes), difference between the PMIP4 and PMIP3 ensembles (in °C, bottom). The PMIP4 average is based on the following models: AWIESM-1, AWIESM-2, INM-CM4, MIROC-ES2L, MPI-ESM1.2, and UofT-CCSM4. The PMIP3 average is based on all PMIP3 models, except the GISS-E2-p151 simulation which did not use the PMIP3 ice sheet for its boundary conditions.

675
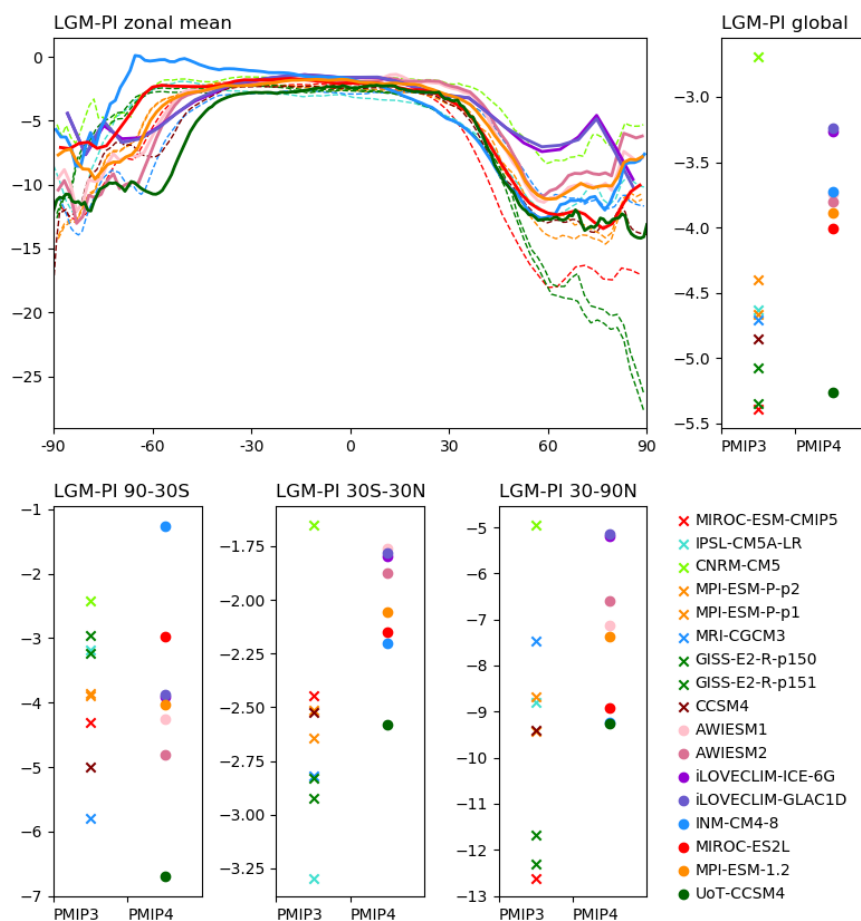
Figure 2: Mean annual temperatures LGM – PI anomalies in °C. Top left: zonal means, PMIP3 model results shown as dashed lines, PMIP4 model results shown as thick solid lines; top right: global means, PMIP3 model results shown by crosses, PMIP4 models shown by filled circles; the three bottom panels show, from left to right, the averages over the southern hemisphere extratropics (90°S to 30°S), the tropics (30°S to 30°N) and the northern extratropics (30°N to 90°N).

Climate
of the Past
Discussions

Open Access

EGU
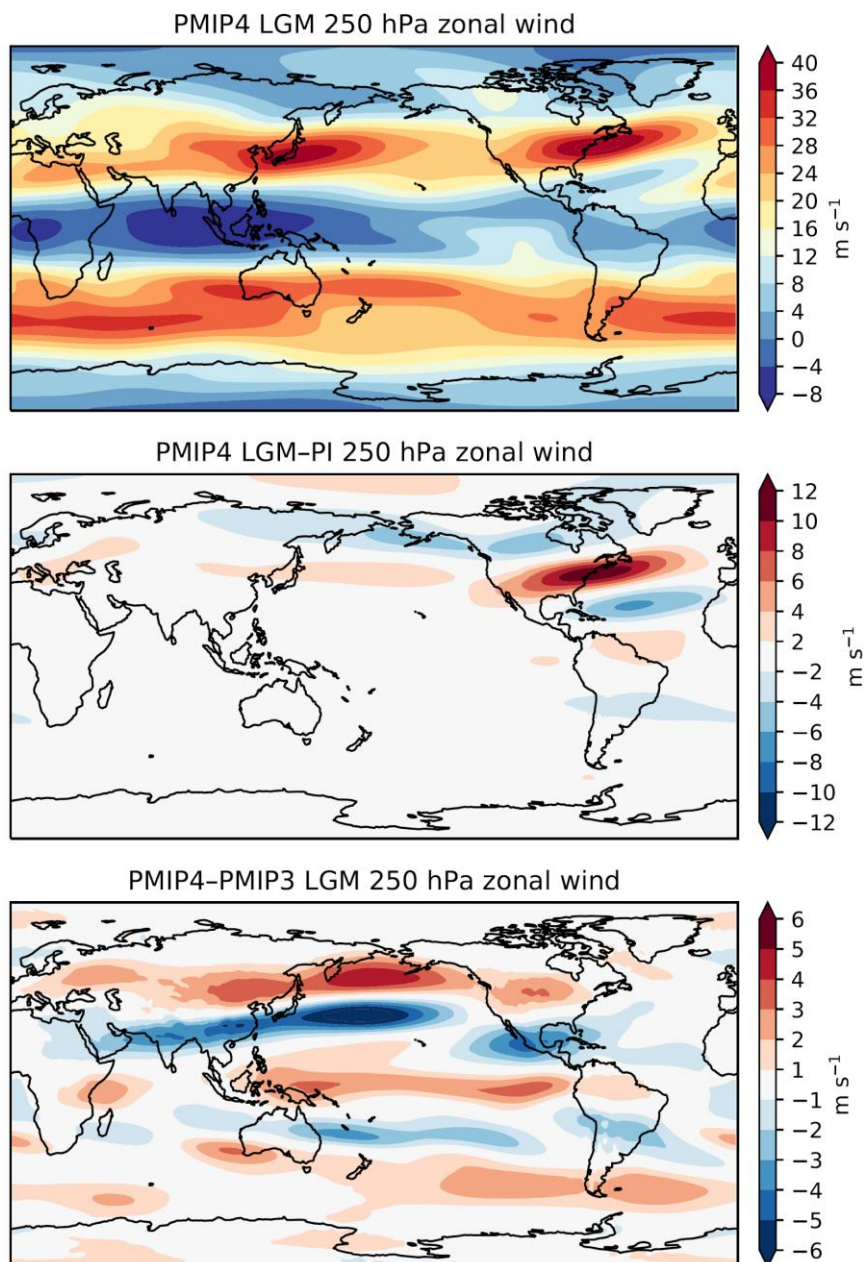
Figure 3: Same as Figure 2 but for the 250 hPa zonal wind. The PMIP4 average is based on the results from AWIESM1, AWIESM2, UofT-CCSM4, MIROC-ES2L, and MPI-ESM1.2. The PMIP3 average is based on all PMIP3 models in Table 1, except the GISS-E2-p151 simulation which did not use the PMIP3 ice sheet for its boundary conditions.

Climate
of the Past
Discussions
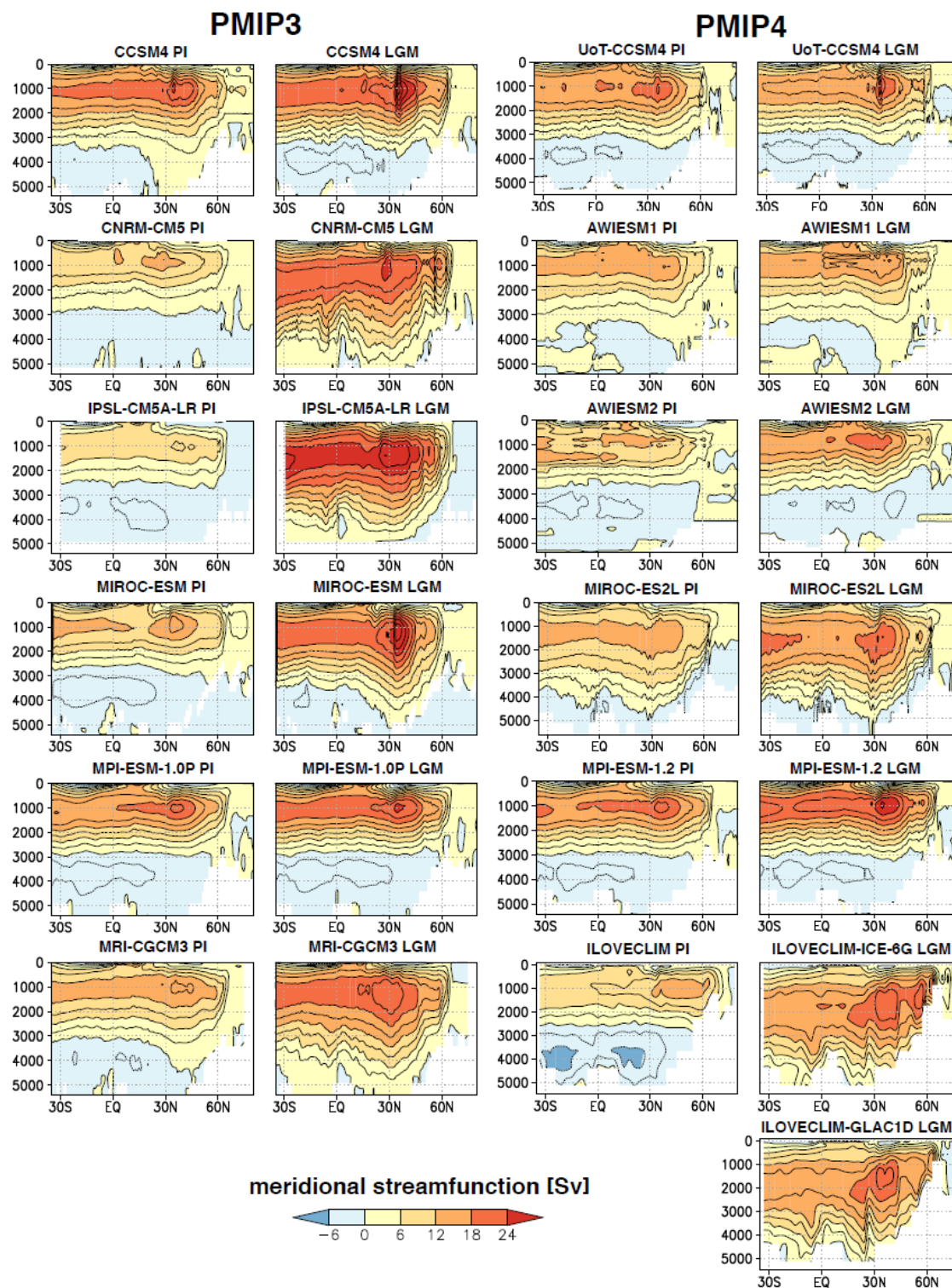
Figure 4: Mean Atlantic Meridional Overturning Circulation simulated by the PMIP3 and PMIP4 models for PI and LGM.
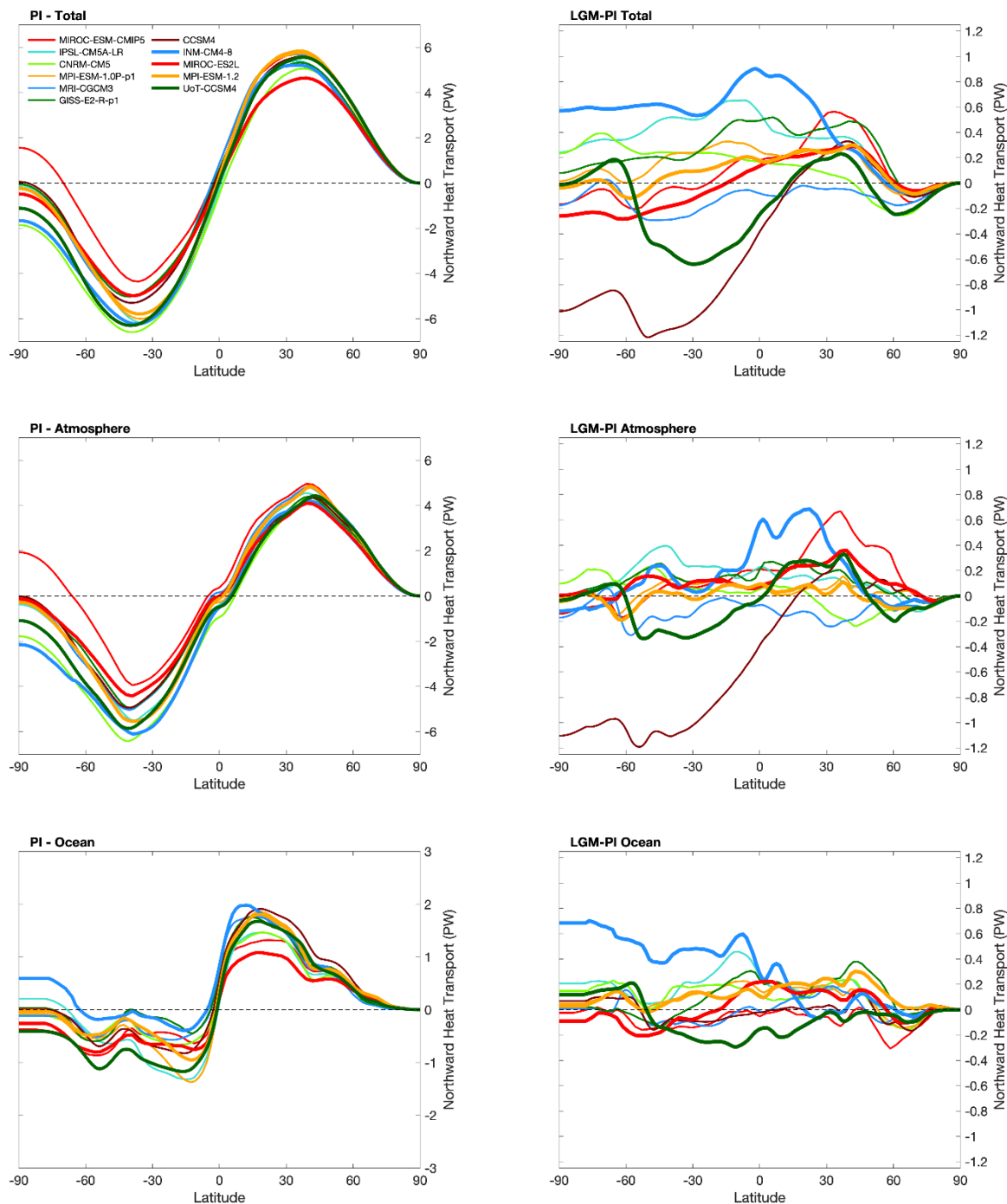
Figure 5: Meridional energy transport for the PI reference state (l.h.s) and LGM - PI anomaly (r.h.s). top: total energy transport, middle: atmospheric energy transport, bottom: oceanic energy transport.
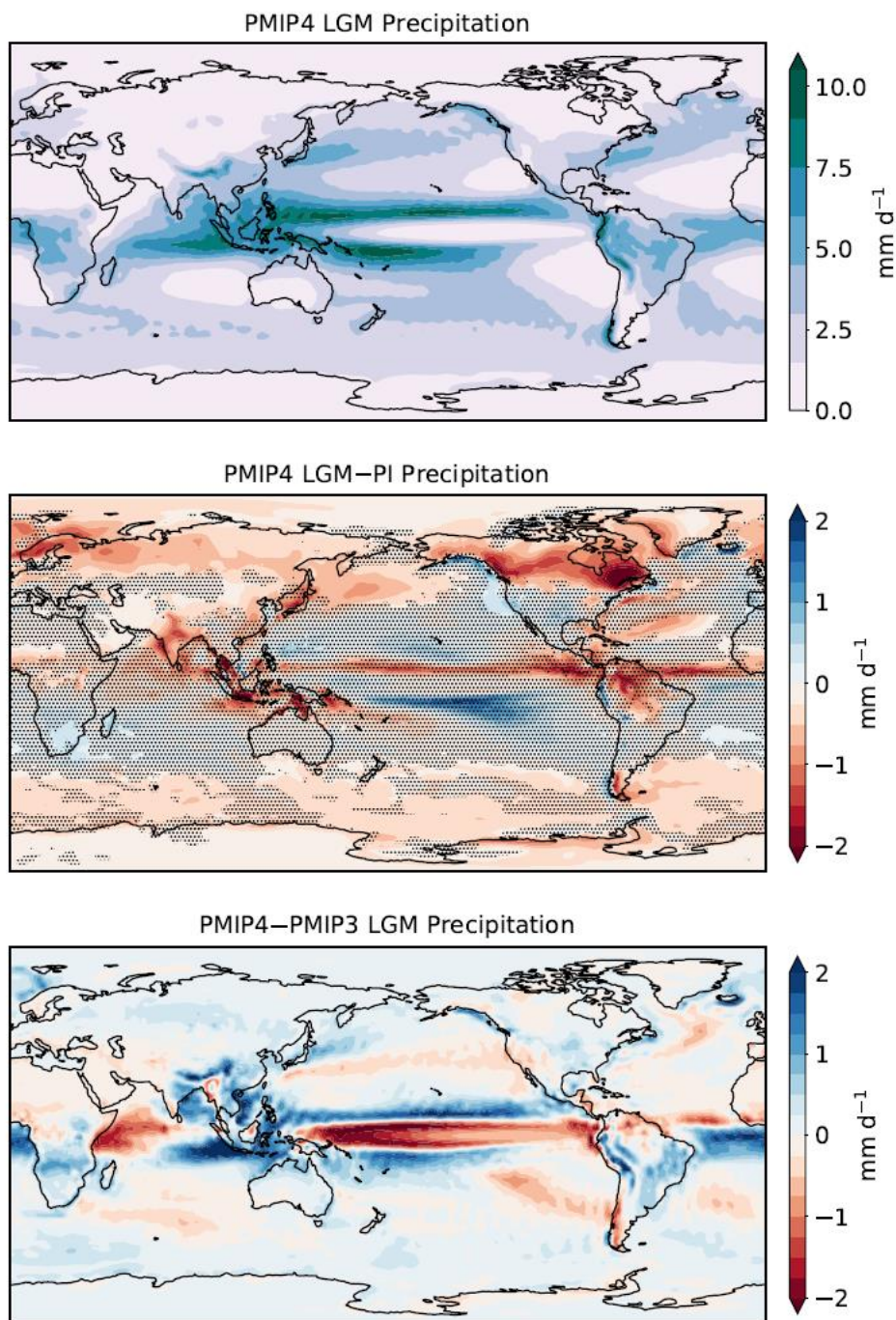
Figure 6: Same as Figure 1 but for mean annual precipitation, in mm/day.
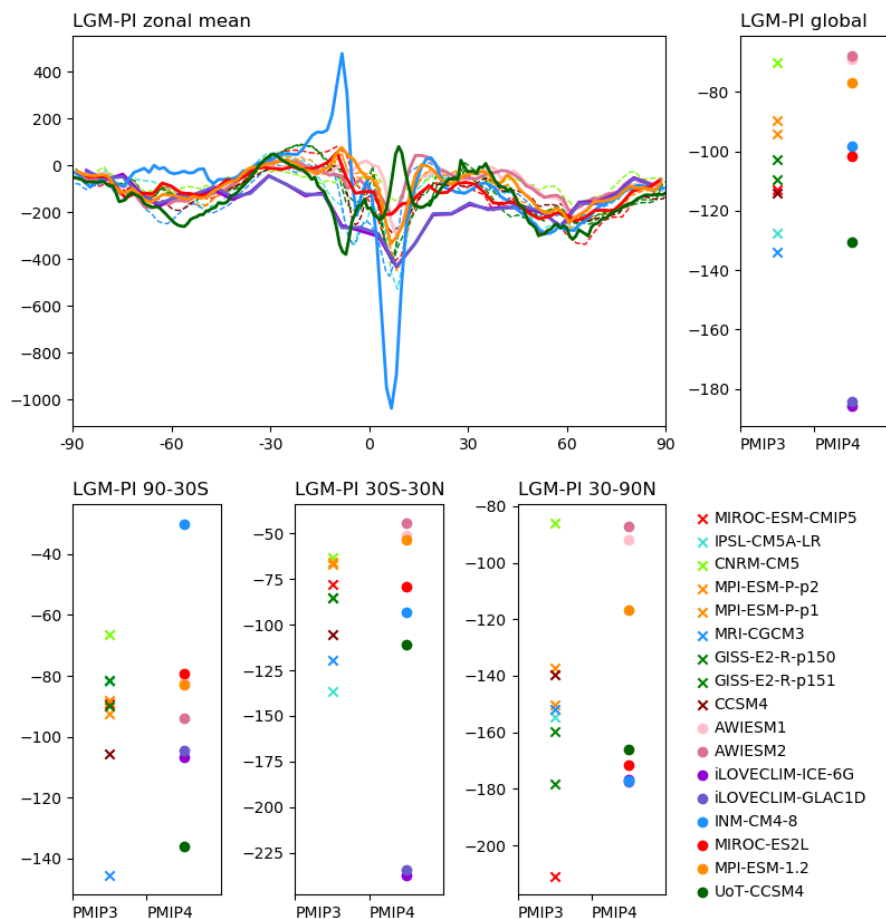
Figure 7: Same as Figure 2 for mean annual precipitation, in mm/year.

Climate
of the Past
Discussions
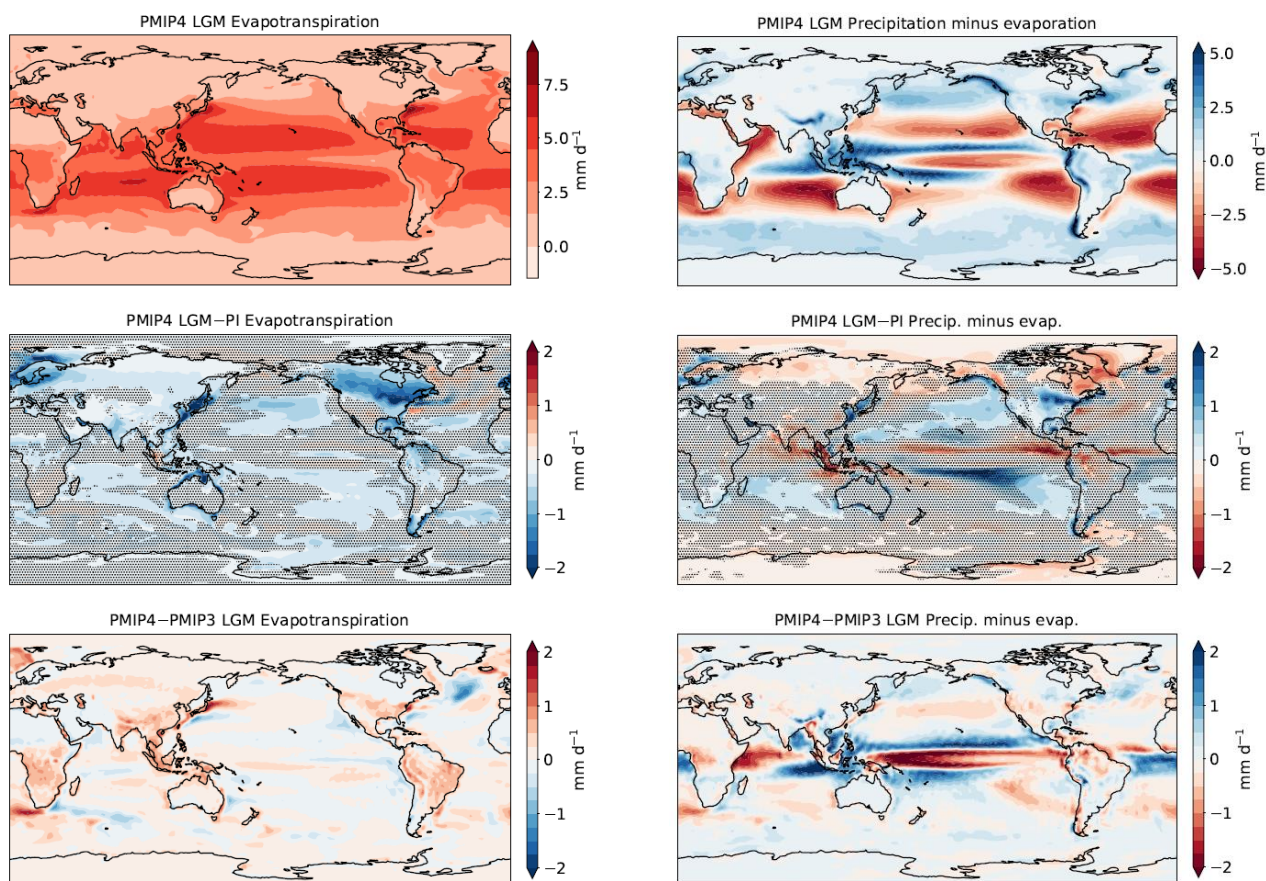
Figure 8: same as Fig. 1 for mean annual evaporation (l.h.s) and mean annual net precipitation (precipitation - evaporation, r.h.s). All values are in mm/day.

705
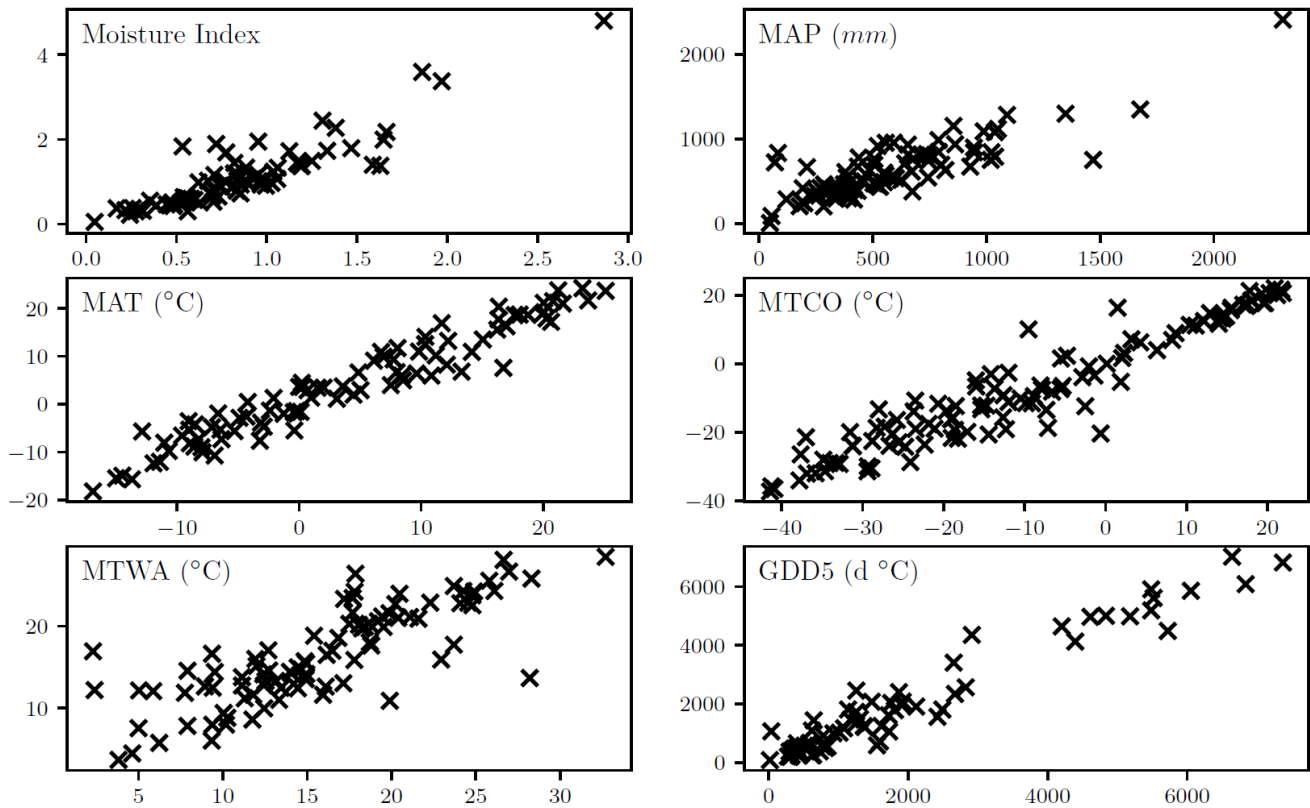
Figure 9: Comparison of terrestrial climate variables from the Bartlein et al. (2011) and the Cleator et al. (2019) reconstructions. The variables are mean annual temperature (MAT), mean temperature of the coldest month (MTCO), mean temperature of the warmest month (MTWA), and growing season temperature indexed by growing degree days above a baseline of 5°C (GGD5), mean annual precipitation (MAP) and an index of soil moisture (Moisture Index). The plots shows comparisons at grid cells that are common between the two data sets.
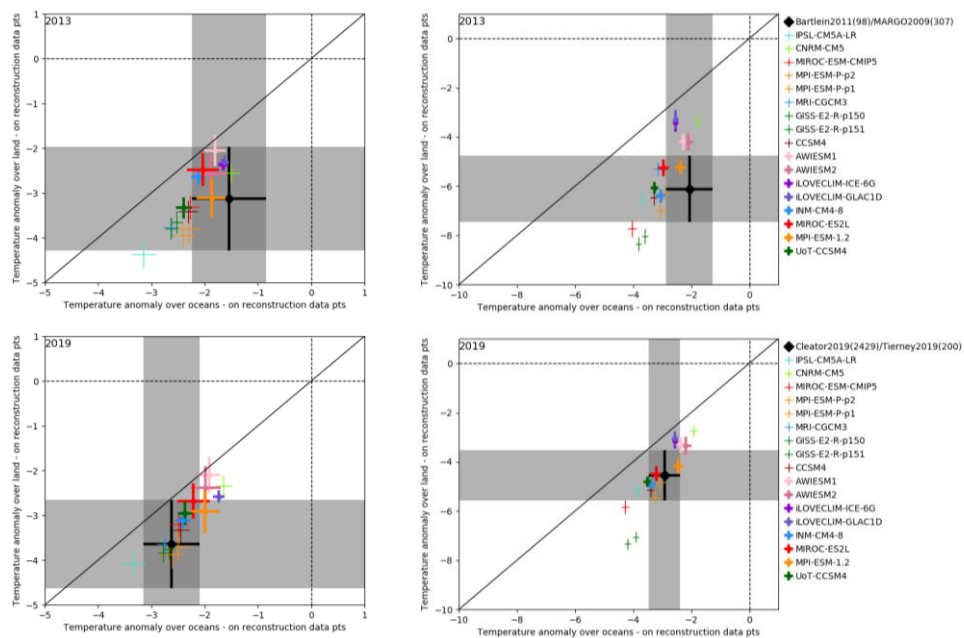
Figure 10: LGM - PI mean annual temperature anomaly over land vs. LGM - PI mean annual temperature anomaly over oceans, averaged over the tropics (30°S-30°N, l.h.s) and over the globe (r.h.s). The model output considered for the averages is taken only on grid points for which there are reconstructions. The top plots are based on the reconstructions used to evaluate the PMIP3-CMIP5 models: the Bartlein et al. (2019) database and the MARGO (2019) SST reconstructions. The bottom plots are based on the most recent reconstructions: Cleator et al. (2019) for terrestrial data and Tierney et al. (2019) for the SSTs.

715
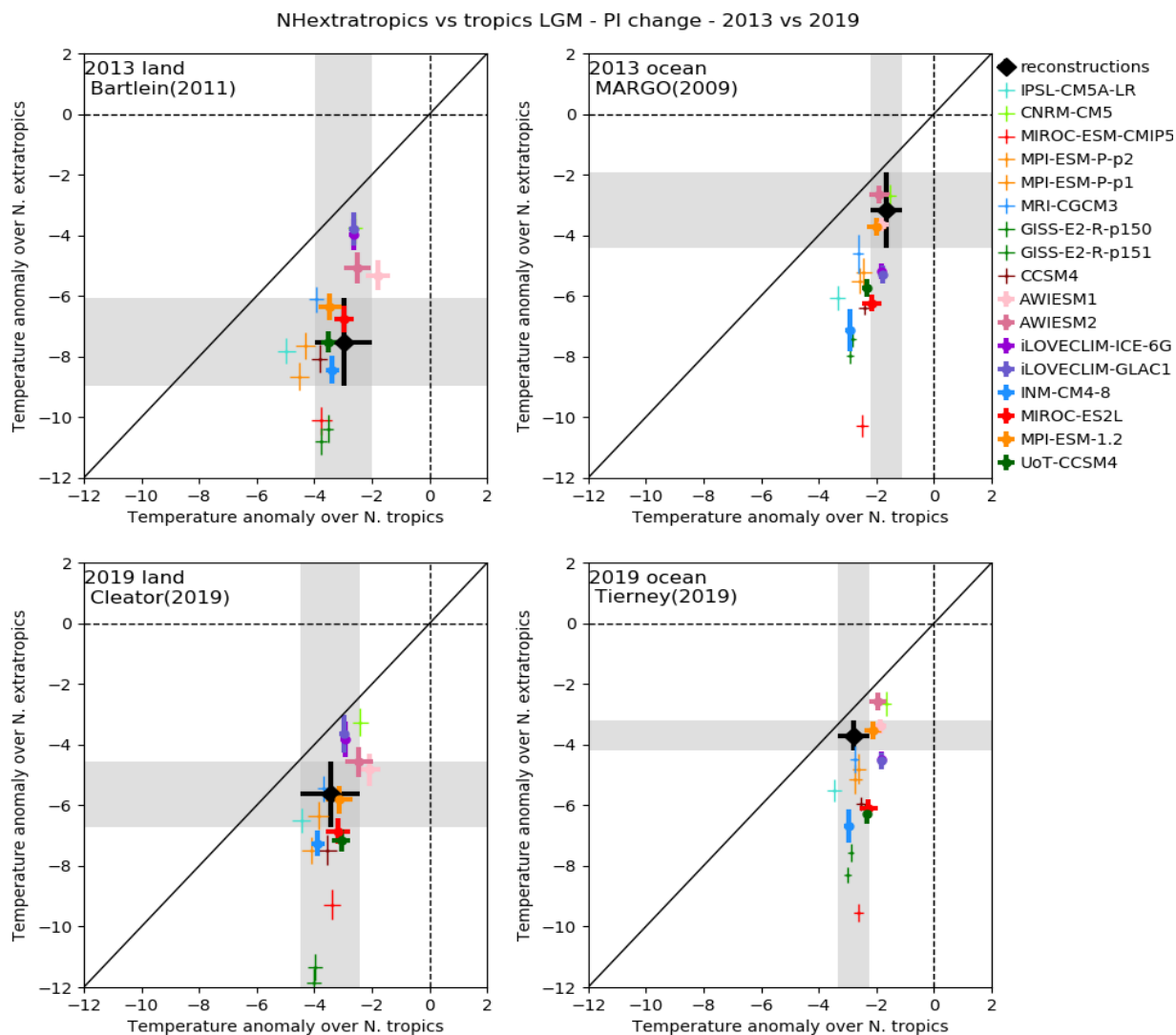
Figure 11: LGM - PI mean annual temperature anomaly over the northern extratopics (30-90°N) vs. over the northern tropics (0-30°N). The model output considered for the averages is taken only on grid points for which there are reconstructions. The four panels are based on the data syntheses of Bartlein et al. (2011) (top left), MARGO (2009) (top right), Cleator et al. (2019), Tierney et al. (2019).

720

725
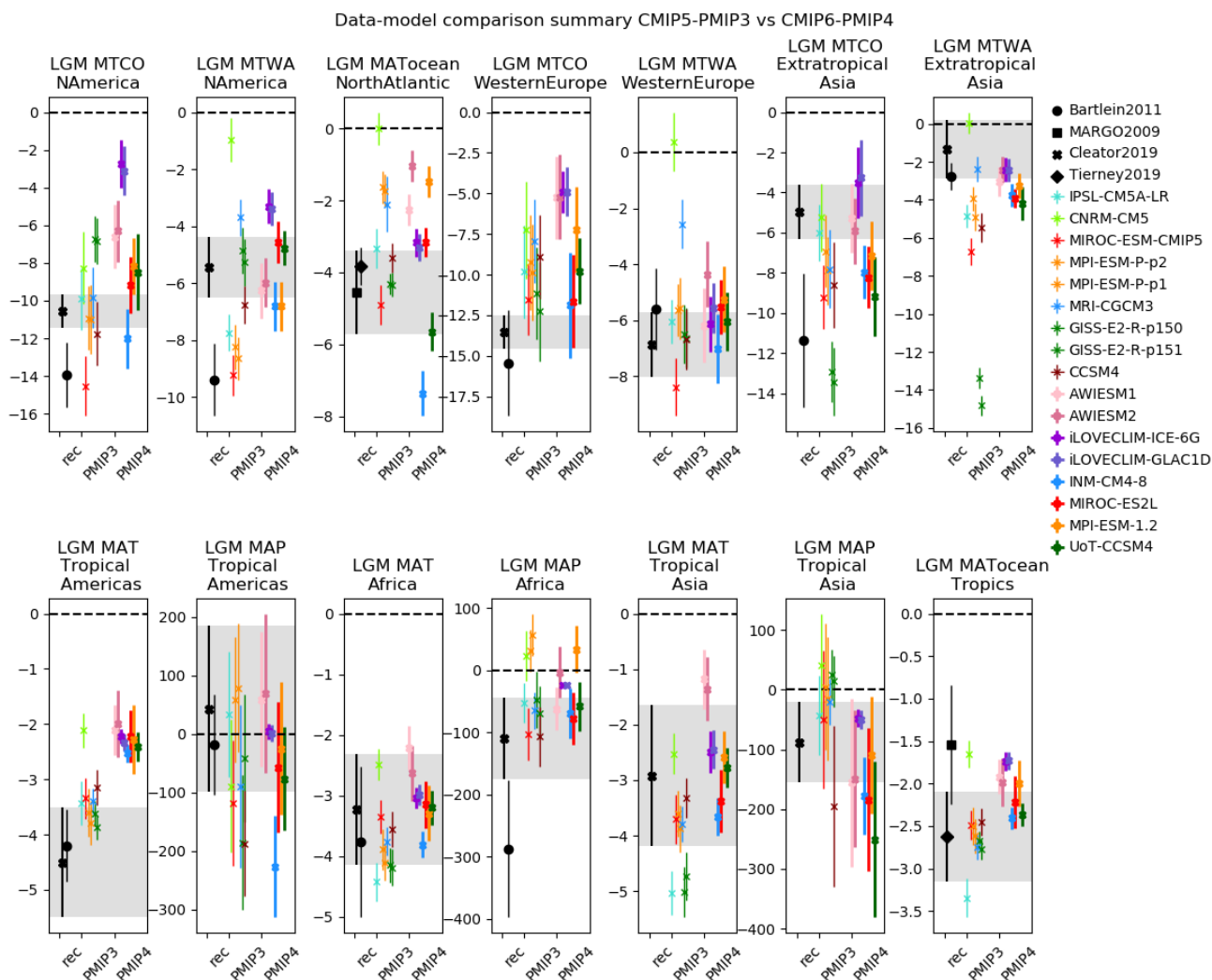
Figure 12: Data-model comparisons for North America (20-50°N, 140-60°W), the North Atlantic Ocean (30-50°N, 60°W-10°W), Western Europe (35-70°N, 10°W-30°E) , Extratropical Asia (35-75°N), Tropical Americas (30°S-30°N, 120-60°W), Africa (35°S-35°N, 10°W-50°E), and tropical oceans (30°S-30°N). MTCO: Mean Temperature of the Coldest Month, MTWA: Mean Temperature of the Warmest Month, MAT: Mean Annual Temperature, MAP: Mean Annual Precipitation, MATocean: Mean Annual Temperature over the oceans The error bars for the reconstructions are based on the standard error given at each site: the average and associated standard deviation over the specific area are obtained by computing 10000 times the average of randomly drawn values in the gaussian distributions defined at each site by the reconstruction mean and standard error, taken as the standard deviation of the gaussian. The error bars for the model results are based on the interannual variability of the average over the area: the mean ± one standard deviation is plotted for each model.
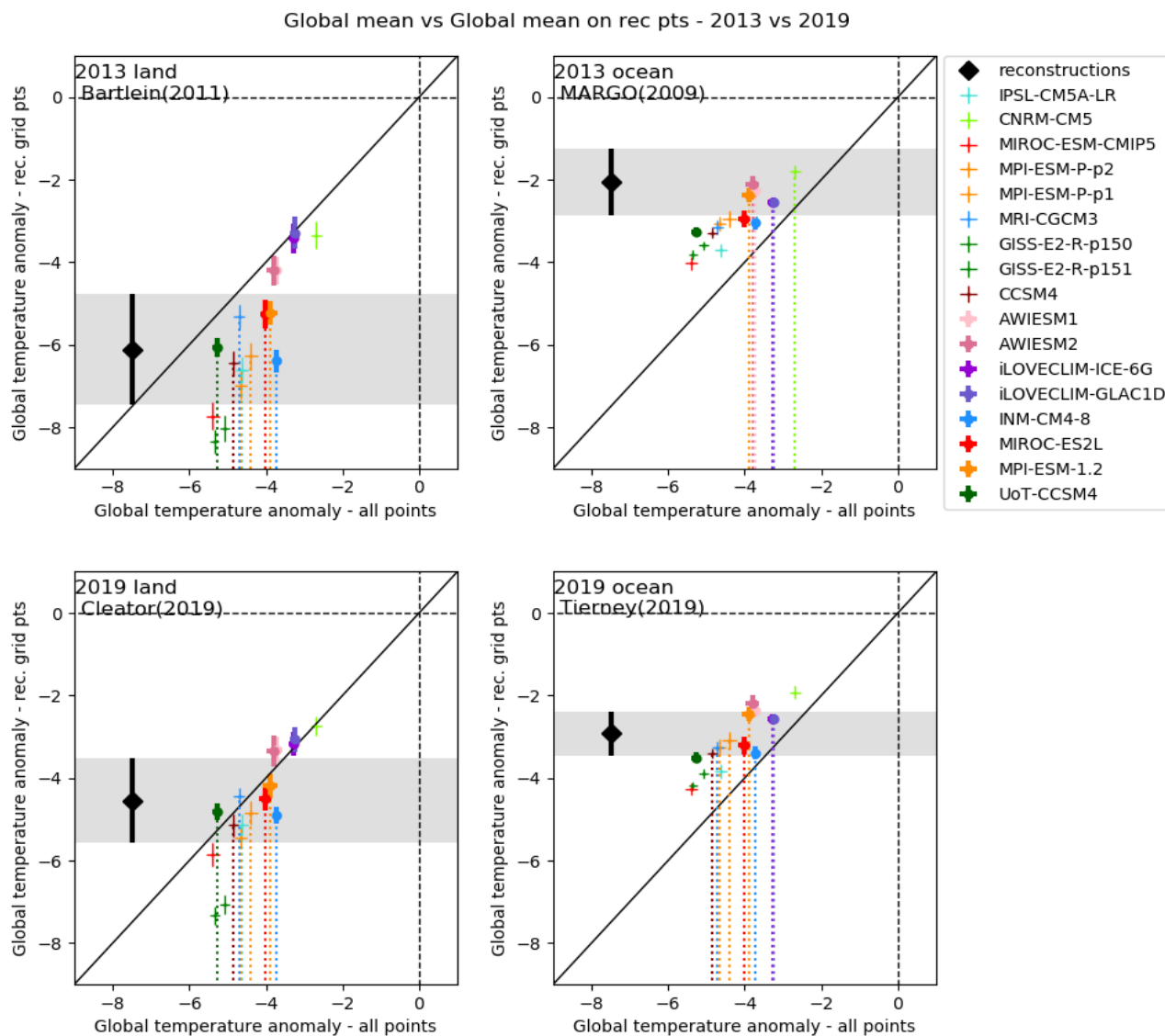
Figure 13: Relationships between global mean temperature changes (x-axes, average computed on all model points) and global mean temperature changes for grid points where there are reconstructions (y-axes, 1 plot per data set). For each plot/data set, the models whose average falls in the range of the average of the reconstructions are marked by vertical dotted lines down to the x-axis.